ERDC/CRREL MP-16-1

US Army Corps
of Engineers®
Engineer Research and
Development Center

ERDC
INNOVATIVE SOLUTIONS
for a safer, better world

Strategic Environmental Research and Development Program (SERDP)

Effect of Arctic Amplification on Design Snow Loads in Alaska

SERDP RC-2435

Kathleen Jones and Steven Daly

September 2016

Cold Regions Research
and Engineering Laboratory

The U.S. Army Engineer Research and Development Center (ERDC) solves the nation's toughest engineering and environmental challenges. ERDC develops innovative solutions in civil and military engineering, geospatial sciences, water resources, and environmental sciences for the Army, the Department of Defense, civilian agencies, and our nation's public good. Find out more at www.erdc.usace.army.mil.

To search for other technical reports published by ERDC, visit the ERDC online library at http://acwc.sdp.sirsi.net/client/default.

Strategic Environmental Research and Development Program (SERDP)

ERDC/CRREL MP-16-1
September 2016

Effect of Arctic Amplification on Design Snow Loads in Alaska

SERDP RC-2435

Kathleen Jones and Steven Daly

U.S. Army Engineer Research and Development Center (ERDC)
Cold Regions Research and Engineering Laboratory (CRREL)
72 Lyme Road
Hanover, NH 03755-1290

Final Report

Prepared for Strategic Environmental Research and Development Program (SERDP)
4800 Mark Center Drive, Suite 17D08
Alexandria, VA 22350-3605

Under SERDP RC-2435

Contents

Tables

Figures

List of Acronyms

80th%	80th percentile
AA	Arctic amplification
ASCE	American Society of Civil Engineers
ASR	Arctic System Reanalysis
CMIP5	Coupled Model Intercomparison Project Phase 5
COOP	Cooperative Observer Program
CRREL	Cold Regions Research and Engineering Laboratory
DOD	Department of Defense
EVA	extreme value analysis
GCM	global climate model
GEV	generalized extreme value distribution
GHCND	Global Historical Climatology Network–Daily
GLO	generalized logistic distribution
GPA	generalized Pareto distribution
HadGEM2-AO	Hadley Centre Global Environment Model Version 2
INM	Institute of Numerical Mathematics
INM-CM4	Institute of Numerical Mathematics Climate Model Version 4.0
LAI	leaf area index
LN3	3-parameter lognormal distribution
MERRA	Modern Era Retrospective analysis for Research and Applications
MRI	mean recurrence interval
NARR	North American Regional Reanalysis
NCDC	National Climatic Data Center
NCEP	National Centers for Environmental Prediction
NRCS	Natural Resource Conservation Service
NSIDC	National Snow and Ice Data Center
NWCC	National Water and Climate Center
NWS	National Weather Service
PASR	Pan-Arctic snow reanalysis
PE3	Pearson Type III distribution
POR	period of record
RCP	Representative Concentration Pathway
SEI	Structural Engineering Institute
SNODEP	daily snow depth analysis by Air Force Weather Agency
SNOTEL	snowpack telemetry
SWE	snow water equivalent
UFC	Unified Facilities Criteria
UTC	Coordinated Universal Time

Keywords: Alaska, Arctic amplification, climate change, extreme value analysis, snow loads, snow water equivalent, SWE

Acknowledgements: This work was conducted with support from the Strategic Environmental Research and Development Program, Project Number 2435. We thank SERDP program manager

Dr. John Hall for his support and insightful questions. We appreciate the help of the U.S. Army Cold Regions Research and Engineering Laboratory's (CRREL) Dr. Christopher Hiemstra in obtaining the data from the Liston and Hiemstra (2011) paper and grid point locations.

Abstract

Objectives

The Department of Defense seeks an improved understanding and capacity to respond to potential climate change impacts on built infrastructure in Alaska. Other studies have hypothesized that Arctic amplification, the rapid warming of the Arctic compared to the northern hemisphere, causes more persistent weather patterns at midlatitudes, which increase the probability of extreme weather due to drought, flooding, cold spells, and heat waves. Annual maximum snow loads, resulting from the accumulation of snow throughout the winter season, may be strongly influenced by persistent weather patterns. We investigated their effect on annual maximum snow loads and the resulting design snow loads for buildings.

Technical Approach

The extent of sea ice is a large-scale symptom of Arctic warming and Arctic amplification (AA). The decrease in the annual minimum Arctic sea ice extent began in 2000, and by 2005 all the minima were less than the pre-2000 minima. Therefore, we use the characteristics of snow load data through the winter of 2003–2004 to be indicative of the conditions prior to AA and the period beginning with the winter of 2004–2005 to be associated with AA.

Design snow loads for buildings are specified for a 50-year return period and are based on an extreme value analysis of the annual maximum snow loads. The snow load can be described in terms of the snow water equivalent (SWE) of the snowpack. We acquired SWE data from a number of sources that provide automatic or manual observations, reanalysis data, or modeled snow accumulation using downscaled reanalysis data. For each dataset, we determined the maximum SWE for each year at each location and compiled the characteristics of the winter up to the day with the maximum snow accumulation.

The periods of record of the datasets are short, particularly when they are separated into two eras. The records might include, just by chance, years with large snow loads or might have only ordinary loads. This sampling error is reflected in the results of an extreme value analysis. Extremes obtained from long periods of record are more reliable. Therefore, we used the characteristics of the snow accumulation seasons to generate years of synthetic accumulation seasons. For each location, we calculated the correlation of the annual maximum SWE with parameters characterizing the accumulation season. The short records also provide little data to define the distributions of these parameters. Therefore, we used the chi-square test to compare the distributions of the daily SWE increment at each location with the other locations. For locations where the probability that the distributions were the same was high, we merged those daily SWE increments. Two-thirds of the locations had at least one other locations with a SWE increment distribution that was similar. We used the expanded set of characteristics of the snow accumulation seasons to generate synthetic seasons, choosing values for each day from the distribution of the daily SWE increments for that location. Each winter was characterized by two randomly chosen values of parameters correlated with the annual maximum SWE.

In the extreme value analysis, we used the regional frequency analysis approach with the long period of record of synthetic SWE as input. L-moments were used to characterize the data and to fit extreme value distributions. Three- and four-parameter extreme value distributions are fit to the data to allow the shape of the tail of the distribution to be defined by the data.

Results

We found that the annual maximum SWE was correlated with the number of days with snowfall and with the 80th percentile (80th %) SWE increment. The location associations based on the chi-square test of the daily SWE increment also provide an expanded set of 80th% SWE increments. To expand the set of the number of days with snowfall, we compared the distribution of this parameter at each location with the other locations by using the Kolmogorov-Smirnov test. At each location, the distributions of the number of days with snowfall and the 80th% SWE increment were separated into two groups: on the pre-AA era and the AA era. We used these expanded sets of characteristics of the snow accumulation seasons to generate synthetic winters, randomly choosing values for each day from the distribution of the daily SWE increments. Each winter is characterized by the number of days with snowfall and 80th% SWE increment, each chosen randomly. For each location in each era, we generated 499 winters of SWE to use in the extreme value analysis. The calculated 50-year snow loads are typically not significantly different between the pre-AA era and the AA era. For the dataset based on observed SWE, snow loads that were different tended to be lower in the AA era. For the two datasets based on reanalysis data, loads that were different tended to be higher in the AA era.

We also did a running extreme value analysis of twenty-first century simulations from two global climate models, analyzing 33-year-long blocks of data moved in 10-year increments. The British model indicated increasing SWE in the north and decreasing in the south with the magnitude of the trend increasing with greater total radiative forcing. The Russian model showed smaller trends with the increasing trend in the north reversing with greater total radiative forcing.

Benefits

This analysis indicates that changes in design snow loads in Alaska associated with global climate change are not justified by the available data or by simulations of future climate. Redoing the analysis in 10 or 20 years with a longer period of record of SWE data would be useful. Until then, the snow load guidance that is available in national standards and the Uniformed Facilities criterion website continues to be applicable. This study has pointed out the dearth of information on design snow loads in Alaska compared to the lower 48 states. Alaska is a huge state with great variation in terrain and climate over short distances and snow load measurement sites are few and far between. Therefore, standards provide design snow loads for only a few locations in Alaska. The investigation of SWE datasets to use for this project has shed light on some of the issues around measured SWE. At most first-order weather stations on most days, SWE is estimated by dividing the snow depth by ten, rather than measured. Thus, any apparent daily variation in the reported SWE may not be real. Reanalysis products assimilate those measurements and the measurements are also used in validating satellite observations and global climate model simulations of SWE.

Objectives

The Department of Defense (DOD) seeks an improved understanding and capacity to respond to potential climate change impacts on built infrastructure, including buildings, in Alaska and in similar climates. In this project, we explore potential changes in design snow loads in a climate with more persistent winter weather patterns. The rapid warming of the Arctic compared to the entire northern hemisphere is termed Arctic amplification (AA) (Serreze and Barry 2011). Francis and Vavrus (2012) relate AA to two mechanisms that may cause more persistent midlatitude weather patterns. The first mechanism is a reduced south-to-north gradient in the difference between the 1000 and 500 mb atmospheric heights, which in turn weakens the upper-level zonal flow. This causes the circulation systems to move more slowly. The second mechanism is the elongation of ridge peaks at the 500 mb level, which amplifies the trajectory of the flow. This amplification increases the probability of slow eastward progression of large-scale weather patterns. Both of these effects tend to cause more persistent weather patterns at mid-latitudes, which increase the probability of extreme weather due to drought, flooding, cold spells, and heat waves. Note that midlatitudes in the northern hemisphere extend from the Tropic of Cancer to the Arctic Circle. Annual maximum snow loads in Alaska, resulting from the accumulation of snow throughout the winter season, may be strongly impacted by persistent weather patterns. In this project, we investigated the possible effects of these persistent weather patterns on annual maximum snow loads and the resulting design snow loads for infrastructure. The design snow loads for built infrastructure are obtained from the annual maxima by an extreme value analysis (EVA) of the annual maximum snow loads.

Background

Arctic Amplification and Persistence

We expect a greater variance in snow loads from year to year when circulation patterns persist during a winter, and this variance in turn affects the shape of the tail of the extreme value distribution. In another Arctic application, Dr. Matthew Sturm and Dr. Michael Goldstein found that the crucial factor affecting the use of ice roads in the Northwest Territories of Canada is not the trend in climate data but the variance in freezing degree-days (Sturm 2012). Variance is important in that case because it alters the risk–benefit calculation that is crucial to business decisions.

The extent of sea ice is a large-scale symptom of Arctic warming and AA. The decrease in the annual minimum Arctic sea ice extent began in 2000 (Figure 1) (NSIDC 2016). However, it was not until 2005 that the minima were less than all the pre-2000 minima. Therefore, in this study, we use the characteristics of snow load data through the winter of 2003–2004 to be indicative of the conditions prior to AA and the period beginning with the winter of 2004–2005 to be indicative of the conditions associated with AA.

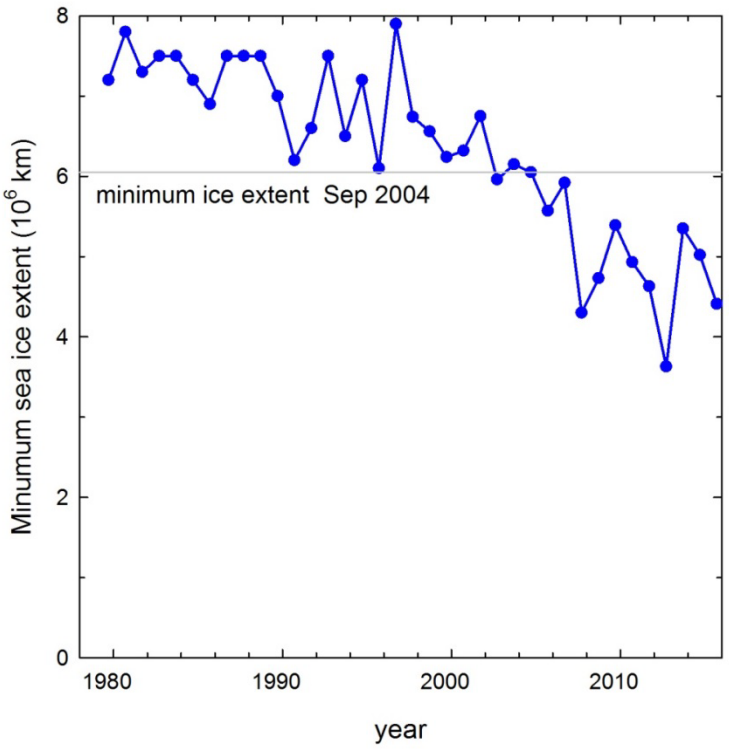

Figure 1. Minimum Arctic sea ice extent 1978–2015. All minimum ice extents after 2004 are less than all ice extents through 2000.

Snow Loads and Extreme Value Distributions

In the United States, design snow loads for buildings are provided in the "Snow Loads" chapter of the American Society of Civil Engineers (ASCE) Standard 7, *Minimum Design Loads for Buildings and Other Structures* (ASCE 2010). These loads are based on an EVA of the annual maximum ground snow loads. The snow load can be described in terms of the snow water equivalent (SWE) of the snowpack. SWE is the depth of water that would be obtained by instantaneously melting the entire snowpack. SWE divided by the specific gravity of the snow is the snow depth. SWE (units of meters or feet) multiplied by the density of water (1000 kg/m^3 or 62.4 lb/ft^3) is the snow load (kg/m^2 or lb/ft^2). The observed annual maxima of SWE at a location are used to determine the extreme value distribution of SWE at that location. SWE for any mean recurrence interval (MRI) are obtained from this distribution. Values for a 50-year MRI (2% annual exceedance probability) are mapped in ASCE (2010), which also includes a table to estimate SWE for other MRIs from the 50-year values. The mapping increment for 50-year snow loads is 5 lb/ft^2, which is a SWE increment of 1 in. Snow loads for Alaska are not mapped. Instead, a table of values for 33 locations in the state is provided with values ranging from 25 to 300 lb/ft^2 (5 to 58 in. SWE). The Commentary to the chapter explains that those values are for the specific locations only and should not be used for nearby locations. It goes on to say that the table is provided to exhibit the large spatial variability in snow loads in Alaska.

Guidance is provided in the "Snow Load" chapter and associated Commentary for obtaining design roof snow loads with a 50-year MRI from the ground snow loads. Multiplicative factors in the "Combinations of Loads" chapter effectively specify a design snow load that has an MRI of hundreds of years for buildings with an ordinary Risk Category. There are higher Risk Categories for buildings that are essential facilities; buildings whose failure would pose a substantial risk to people; and buildings used to process, store, or dispose of hazardous materials. Buildings in these Risk Categories are designed for snow loads with even longer mean recurrence intervals.

In the online Unified Facilities Criteria (UFC), which follows ASCE (2010) Standard 7, the DOD provides design loads for structures. The UFC system is administered by the U.S. Army Corps of Engineers, the Naval Facilities Engineering Command, and the Air Force Civil Engineer Center. Ground snow loads for a 50-year MRI are provided in Table E2 of DOD (2014) for seven military bases and four cities in Alaska. The loads range from 30 to 170 lb/ft^2 (6 to 33 in. SWE).

Snow loads with a 50-year mean recurrence interval mapped in ASCE (2010) Standard 7 are based on the two-parameter lognormal distribution (Ellingwood and Redfield 1983). Wind extremes and icing extremes in that standard are described by the two-parameter Gumbel distribution and the three-parameter generalized Pareto distribution, respectively. There are a number of three-parameter distributions that tend to conform better to samples of extremes than the Gumbel distribution. These include the generalized extreme value, generalized logistic, and Pearson Type III distributions (Hosking and Wallis 1997). These distributions may have tails like the normal or Gumbel distribution (tail shape parameter $k = 0$), finite tails ($k > 0$), and long (or thick) tails ($k < 0$) (Figure 2). The two-parameter lognormal distribution also represents this variety of tail shapes. The corresponding three-parameter distribution adds a location parameter and uses a parameterization that includes the normal distribution as a special case (Hosking and Wallis 1997).

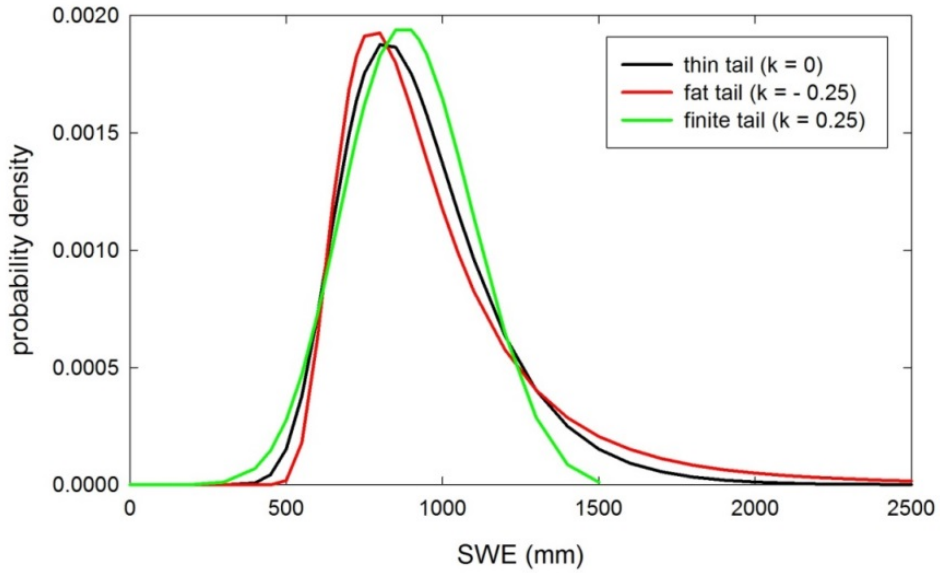

Figure 2. Tail shapes for the generalized extreme value distribution for $k < 0$ (long tail), $k = 0$ (short tail), and $k > 0$ (finite tail).

A variable described by a distribution with a finite tail has an upper bound. For example, non-tornadic winds may be described by a distribution with a finite tail because it is physically impossible for winds to exceed, say, 500 mph. If the physical limit is much greater than measured values or if there is no physical limit, then the fitted extreme value distribution may have a short or long infinite tail. Loads that result from accumulating material depend on both the intensity of each event in the accumulation period and the duration of the accumulation period. Snow loads, which accumulate throughout the winter season in cold climates, and ice loads, which accumulate over the duration of freezing rain storms, are examples of this kind of load. Extraordinary loads may result from the accumulation of ordinary amounts of ice or snow over a long period of time. The shape of the tail of the fitted extreme value distribution of the SWE at a location will be determined by the history of observed accumulated annual maximum SWE.

Snow Accumulation Season

Daily values of SWE are available from datasets of measured SWE at specific locations and as gridded data from reanalysis datasets or Global Climate Models (GCMs). The observed daily changes in SWE over the course of a winter reflect the daily snowfall (or rain on snow) and snow melt during the winter. Examples of SWE data are shown in Figure 3 for Indian Pass, Alaska, for the winters of 1979–1980 and 2010–2011. Our focus is on the accumulation portion of the record, beginning with the first snowfall after 1 September and ending on the date with the maximum SWE. That period is shown in red for each winter. In this report, we label the accumulation season with the year at the end of the winter because the maximum SWE occurs in that year. Thus the accumulation season for the winter of 2010–2011 is called 2011.

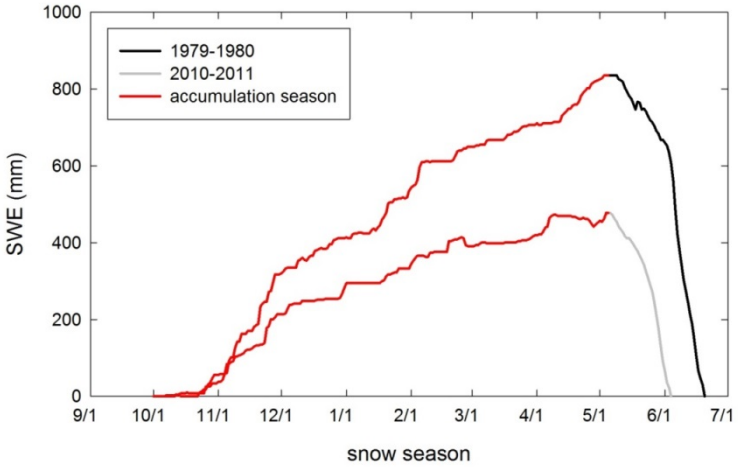

Figure 3. Two winters at Indian Pass, Alaska, showing the daily variation in SWE on the ground. The accumulation season from 1 September to the maximum SWE is shown in *red*.

While there was much less snow in 2011 than in 1980 at Indian Pass, this is not indicative of a general trend at Indian Pass or generally in Alaska. Anchorage, for example, had an all-time record total snow fall in 2012, according to an article on 7 April 2012 in the *Alaska Dispatch*

(Adams 2012). The previous record of 133 in. of snow, compared to the normal 74 in., had been set in the winter of 1955. Other *Alaska Dispatch* articles discuss the pattern in 2012 of generally higher snowfall across Alaska. In Cordova, which was particularly hard hit, National Guardsman and heavy equipment were brought in to clear snow from roofs and streets.

SWE Datasets

We acquired SWE data for this study from a number of sources providing observations, reanalysis products, snow accumulation modeled using downscaled reanalysis data, or GCM simulations.

Observations

The Natural Resources Conservation Service (NRCS) operates an automated system of 750 SNOTEL (snowpack telemetry) sites that collect snowpack data in the western United States and Alaska (NWCC 2016a). The snow water equivalent is measured periodically throughout each day by a pressure-sensing snow pillow, and the transmitted data is quality assured and controlled by the NRCS (NWCC 2016b) and used to estimate a daily SWE value. The sites are designed to operate unattended for at least a year with batteries that are kept charged by solar panels. The primary purpose of this network is to provide information on the snowpack to water managers in the West where 50% to 80% of the water supply is stored in snow. However, this network is also a valuable resource for ground snow load data for the design of buildings to withstand roof snow loads. The 35 SNOTEL sites in Alaska with daily SWE data have periods of record (POR) ranging from 4 to 36 years with a median of 24 years.

The National Weather Service (NWS) reports snow depth and SWE daily at 22 weather stations in Alaska, shown in Figure 5 along with the 35 SNOTEL sites and the military bases. SWE data through 1996 is included in a set of Cooperative Summary of the Day CDs published by the Climate Services Division of the National Climatic Data Center (NCDC). By comparing the measured snow depth to the reported SWE, we found that for many of the Alaska weather stations SWE was typically not measured but estimated by dividing the snow depth by ten. At the eight locations where SWE was often measured rather than estimated, we obtained SWE and snow depth data for the POR from the Global Historical Climatology Network–Daily (GHCND) dataset (Menne et al. 2012a, 2012b). The NWS depths are reported in whole inches and SWE to tenths of an inch. GHCND data is archived in millimeters (depth) and tenths of millimeters (SWE). We converted to the original inches and tenths before analyzing the data.

Reanalysis Products

The North American Regional Reanalysis (NARR) data (Mesinger 2006; NCEP et al. 2005) begins in January 1979 and is updated monthly. Parameters are provided every 3 hours on a Lambert conformal conic grid with a 32 km spacing. The NARR grid over Alaska is shown in Figure 4. NARR is updated daily at the 0000 UTC (Coordinated Universal Time) analysis time from the daily global (47 km) SNODEP (daily snow depth analysis of the U.S. Air Force Weather Agency). According to Gayno et al. (2007), SNODEP's global snow analysis uses microwave-based detection algorithms, snow depth reports, and climatology to produce daily

snow depths on a 47 km grid. Analysts then use satellite imagery to adjust the analysis every day in the Northern Hemisphere. A 5:1 snow-depth-to-SWE ratio is assumed, resulting in twice the SWE that the NWS 10:1 estimate provides for a given snow depth. After downloading data through January 2014 for the entire NARR domain, we saved the data for the portion of the grid that covers Alaska. From that we extracted NARR data at 0000 UTC at the grid locations closest to the SNOTEL, NWS, and military installation locations. There are 67 NARR grid points corresponding to the 7 military locations, 19 of 22 NWS sites, and 35 SNOTEL sites shown in Figure 5. There are no nearby NARR points on land and therefore no SWE data for the NWS weather stations at St. Paul Island, Shemya, and Annette. For six of the sites in complex terrain, an alternate NARR grid point is included. Thirteen of the sites have the same NARR grid point as other sites, so there are 54 unique NARR points. NARR SWE is reported to 0.01 mm. We converted to inches, rounding to the nearest 0.1 in. to have values similar to the SNOTEL and NWS measurements. We corrected the NARR data to remove any large daily increments (many inches) that are followed by an identical increment with the opposite sign on the next day.

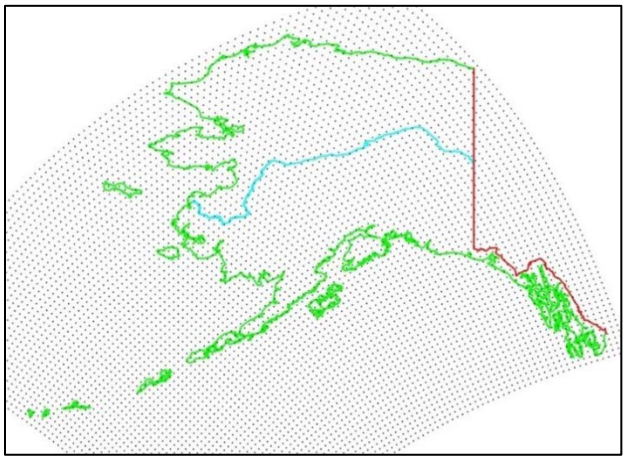

Figure 4. NARR grid over Alaska

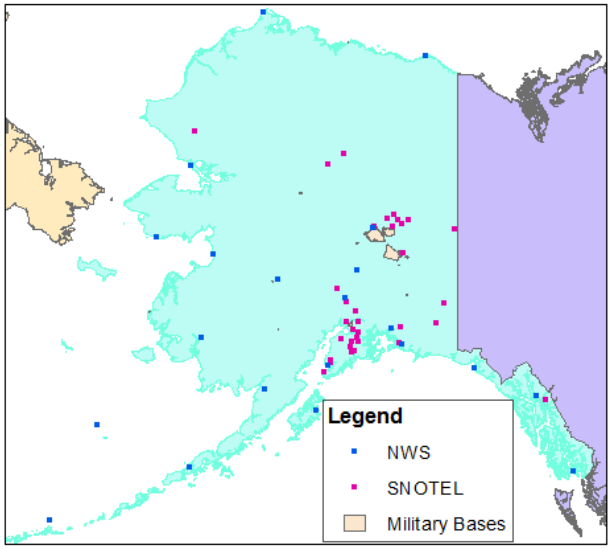

Figure 5. Alaska SNOTEL sites, NWS stations reporting SWE, and military bases.

Modeled SWE Based on Reanalysis Data

We had originally planned to also analyze the 15 km Arctic System Reanalysis (ASR) data from Ohio State University (Bromwich et al. 2014). However, there were significant delays in the generation of that data. In October 2014, there had been no change in the information on the Arctic Systems Reanalysis web site (Polar Meteorology Group 2016) on the availability of the 15 km version of ASR following the website post on April 2014 stating that it was in progress. Given the time constraints on this study, we decided then to use a different dataset. As of January 2016, the 15 km ASR appeared to be still not available. The most recent message on the ASR website, dated July 2015, mentions a target completion date of October 2015 for the 15 km version covering 1 January 2000 to 31 December 2012.

Instead of using SWE from ASR, we are using the Pan-Arctic snow reanalysis (PASR) described in Liston and Hiemstra (2011). These data are on a 10 km grid using Micromet (Liston and Elder 2006b) weather data downscaled from the Modern Era Retrospective analysis for Research and Applications (MERRA) (Rienecker et al. 2011) and then using SnowModel (Liston and Elder 2006a) to generate daily SWE time series from the weather data, taking terrain and vegetation into account. The 30-year POR, beginning with the winter of 1980 and ending in 2009, is available at Earth Observing Laboratory (2016). We worked with Hiemstra to obtain the latitudes and longitudes for the Pan-Arctic grid and extracted SWE time series for the PASR grid points closest to the SNOTEL sites, NWS stations, and military bases.

Global Climate Models

We also obtained daily SWE data for Alaska for two of the Coupled Model Intercomparison Project Phase 5 (CMIP5) GCMs (HadGEM2-AO and INM-CM4) for Representative Concentration Pathways (RCP) 4.5 and 8.5 by using the Earth System Grid Federation data portal hosted by Lawrence Livermore National Laboratory (2016). This data portal has been in the process of redeployment since August 2014 and was expected to be up and running no sooner than mid-January 2016. These GCMs were chosen because their “analyze and visualize” tool in the previous incarnation of the data portal, which allows users to download data for a specified region, was available and working correctly. That tool was either not available or did not work for all the other GCMs with daily SWE data. HadGEM2-AO is the British Hadley Centre Global Environment Model Version 2 with a coupled atmosphere-ocean configuration (Met Office 2016). It is an atmospheric GCM with a grid spacing of 1.875° longitude and 1.25° latitude. At 55° N (approximate latitude of Annette and Cold Bay, Alaska), the resolution is 120 km by 139 km. INM-CM4 is the Russian Institute of Numerical Mathematics (INM) Climate Model Version 4.0. The spatial resolution is 2° longitude by 1.5° latitude. RCP refers to the value of the global radiative forcing in W/m^2. For RCP 4.5, the total radiative forcing rises to 4.5 W/m^2 by about the year 2150 and remains stable after that. For RCP 8.5, the total radiative forcing rises to about 8.5 W/m^2 by the year 2100 and ultimately to about 12.5 W/m^2 by about 2250 (Meinshausen et al. 2011).

How realistic are these two GCMs? The distance metric in Figure 3 in Knutti et al. (2013) that takes into account precipitation and temperature for the CMIP5 GCMs indicates that two of the models in the Hadley family agree better with observations than INM-CM4, which has the

poorest results of the models in that study. This may mean that HadGEM2-AO also agrees significantly better with observations than INM-CM4, but not necessarily. For example, the four GCMs included from the Geophysical Fluid Dynamics Laboratory at Princeton show a wide variation in their agreement with observations.

Materials and Methods

Analysis of SWE Data

In this section, we first describe the SNOTEL, NWS, NARR, and PASR SWE data and our analysis of that data for the purpose of generating synthetic data with the same essential statistics. The four datasets have different characteristics, as shown by the cumulative distributions of the daily SWE increments during the accumulation season in Figure 6. NWS daily ΔSWE range from −6.2 to 11.2 in., and NARR values cover an even wider range from −31.8 to 9.4 in. The SNOTEL and PASR data show few large negative and positive ΔSWE compared to the NWS and NARR data, with ranges from −3.6 to 4.2 in. and −2.8 to 5.2 in., respectively. There are relatively few days in the accumulation season with ΔSWE = 0 in the NARR dataset compared to the other three datasets.

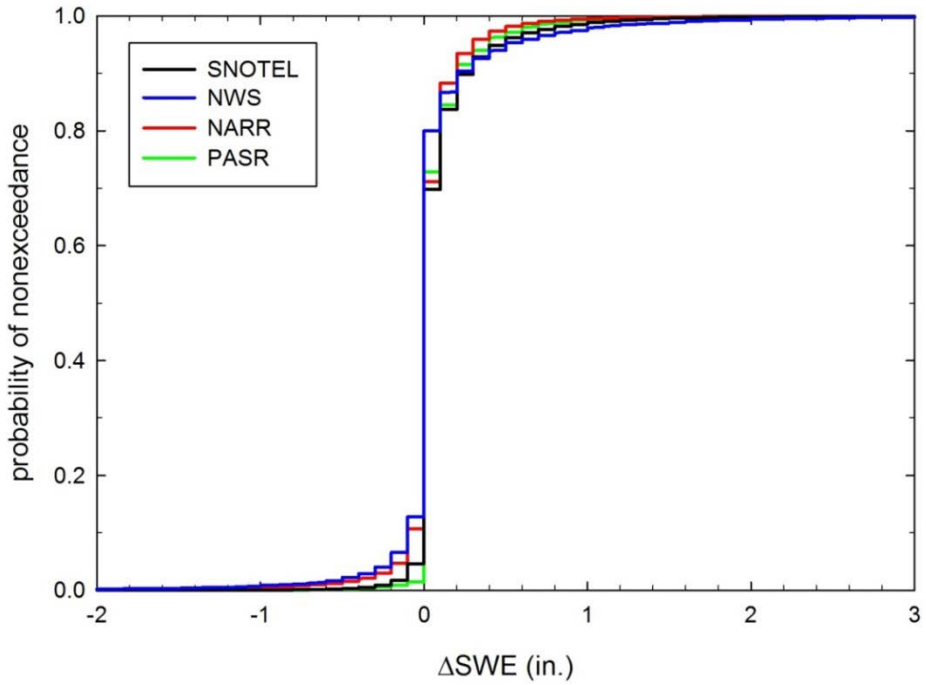

Figure 6. Comparison of daily ΔSWE distributions during the accumulation season for the SNOTEL, NWS, NARR, and PASR data.

We use the characteristics of these datasets to create synthetic data for long POR with the characteristics of the measured SNOTEL, NARR, and PASR SWE data. Our ultimate goal is to use the synthetic data to determine if extreme snow loads in the AA era with greater persistence in weather patterns are different from extremes in the pre-AA era. In the EVA of the synthetic data, we follow the regional frequency analysis approach of Hoskings and Wallis (1997).

SNOTEL

We acquired daily SWE data for the 35 SNOTEL sites in Alaska where SWE is measured for the POR through the winter of 2015. Table 1 lists the sites, with site name and number, location, elevation, county, and POR, organized by county and site number. Figure 7 shows the POR with a vertical line indicating the year 2005, which we are assuming is the beginning of AA and greater persistence in weather patterns.

We computed annual statistics for the accumulation season at each site, based on winter years beginning 1 September and labeled by the end of the winter year. We calculated the correlation of the annual maximum SWE at the SNOTEL sites, using the entire POR, with parameters characterizing the accumulation season, including the duration, number of days with snowfall, e^2-folding lag, and quantiles of ΔSWE on days with snowfall (ΔSWE > 0). The daily ΔSWE may be positive, indicating snowfall or rain on snow; negative, indicating snow melt; or zero. These parameters were chosen because they relate to either the snow load or the persistence of the weather patterns that generate the snow load. The *e*-folding lag, which is the number of days required for the autocorrelation to decrease to $e^{-1} = 0.368$, is often used to characterize autocorrelation. If days with snow tend to be followed by more days with snow, or days with no change in SWE followed by similar days, the *e*-folding lag will be greater than it would be if there is no persistence in the weather from day to day. At these sites, the *e*-folding lag is typically the minimum possible value of 1 day, so we use $e^{-2} = 0.135$, the e^2-folding lag, to provide better discrimination.

In addition to examining the relationships between the maximum SWE and the various accumulation season parameters, we also compared SWE parameters for the periods before AA and with AA. Of the 35 sites, only 27 have more than one winter of data prior to 2005, so a comparison of the mean winter conditions for the two eras is limited to those sites.

We ultimately want to use the characteristics of the available data before and during AA to create synthetic accumulation seasons with similar characteristics for many winters. The short POR at many of the SNOTEL sites provides few examples of accumulation seasons, but we can expand on the data for each site by finding sites with parameters with similar characteristics and by using values from those sites as well. For parameters with values that are binned, we use the chi-square test to compare data samples. For parameters with continuous values, we use the Kolmogorov-Smirnov test. Distributions of samples are generally assumed to be different if the probability that they were drawn from the same population is less than either 5% or 1%. In this application, we are identifying data samples that were likely drawn from the same population, so we set lower limits on the probability. There are no standard values.

Table 1. SNOTEL sites in Alaska, ordered by county and site name.

Name	#	Latitude	Longitude	Elev. (ft)	County	POR
ANCHORAGE HILLSIDE	1070	61.11	−149.67	2080	Anchorage	2006–2015
INDIAN PASS	946	61.07	−149.48	2350	Anchorage	1980–2015
MORAINE	1035	61.38	−149.00	2100	Anchorage	2003–2015
MT. ALYESKA	1103	60.96	−149.09	1540	Anchorage	1973–1973, 1978–2014
FAIRBANKS F.O.	1174	64.85	−147.80	450	Fairbanks N Star	1983–2015
LITTLE CHENA RIDGE	947	65.12	−146.73	2000	Fairbanks N Star	1982–2015
MONUMENT CREEK	949	65.08	−145.87	1850	Fairbanks N Star	1981–2015
MT. RYAN	948	65.25	−146.15	2800	Fairbanks N Star	1982–2015
MUNSON RIDGE	950	64.85	−146.21	3100	Fairbanks N Star	1981–2015
TEUCHET CREEK	951	64.95	−145.52	1640	Fairbanks N Star	1982–2015
UPPER CHENA	952	65.1	−144.93	2850	Fairbanks N Star	1988–2013
LONG LAKE	1001	58.19	−133.83	850	Juneau	1967–1967, 2000–2015
ANCHOR RIVER DIVIDE	1062	59.86	−151.32	1653	Kenai Peninsula	1981–2015
COOPER LAKE	959	60.39	−149.69	1200	Kenai Peninsula	1982–2015
EXIT GLACIER	1092	60.19	−149.62	400	Kenai Peninsula	2012–2015
GRANDVIEW	956	60.61	−149.06	1100	Kenai Peninsula	1992–2015
GROUSE CREEK DIVIDE	964	60.26	−149.34	700	Kenai Peninsula	1998–1998, 2000–2015
KENAI MOOSE PENS	966	60.73	−150.48	300	Kenai Peninsula	1989–2015
MCNEIL CANYON	1003	59.74	−151.25	1320	Kenai Peninsula	1987, 1990–2015
PORT GRAHAM	987	59.35	−151.85	300	Kenai Peninsula	2001–2015
SUMMIT CREEK	955	60.62	−149.53	1400	Kenai Peninsula	1990–2015
TURNAGAIN PASS	954	60.78	−149.18	1880	Kenai Peninsula	1983–2015
INDEPENDENCE MINE	1091	61.79	−149.28	3550	Matanuska-Susitna	2001–2002, 2007–2015
POINT MACKENZIE	1002	61.39	−150.03	250	Matanuska-Susitna	2000–2015
SUSITNA VALLEY	967	62.13	−150.04	375	Matanuska-Susitna	1988–2015
TOKOSITNA VALLEY	1089	62.63	−150.78	850	Matanuska-Susitna	2007–2015
KELLY STATION	1175	67.93	−162.28	310	NW Arctic	1993–1995, 2012–2015
AMERICAN CREEK	1189	64.79	−141.23	1050	SE Fairbanks	2012–2015
CHISANA	1093	62.07	−142.05	3320	SE Fairbanks	2009–2015
GRANITE CREEK	963	63.94	−145.40	1240	SE Fairbanks	1989–2015
MAY CREEK	1096	61.35	−142.71	1610	Valdez-Cordova	2008–2015
MT. EYAK	1073	60.55	−145.75	1405	Valdez-Cordova	2006–2015
UPPER TSAINA RIVER	1055	61.19	−145.65	1750	Valdez-Cordova	2004–2015
BETTLES FIELD	1182	66.92	−151.53	640	Yukon-Koyukuk	1981–2015
COLDFOOT	958	67.25	−150.18	1040	Yukon-Koyukuk	1996–2015

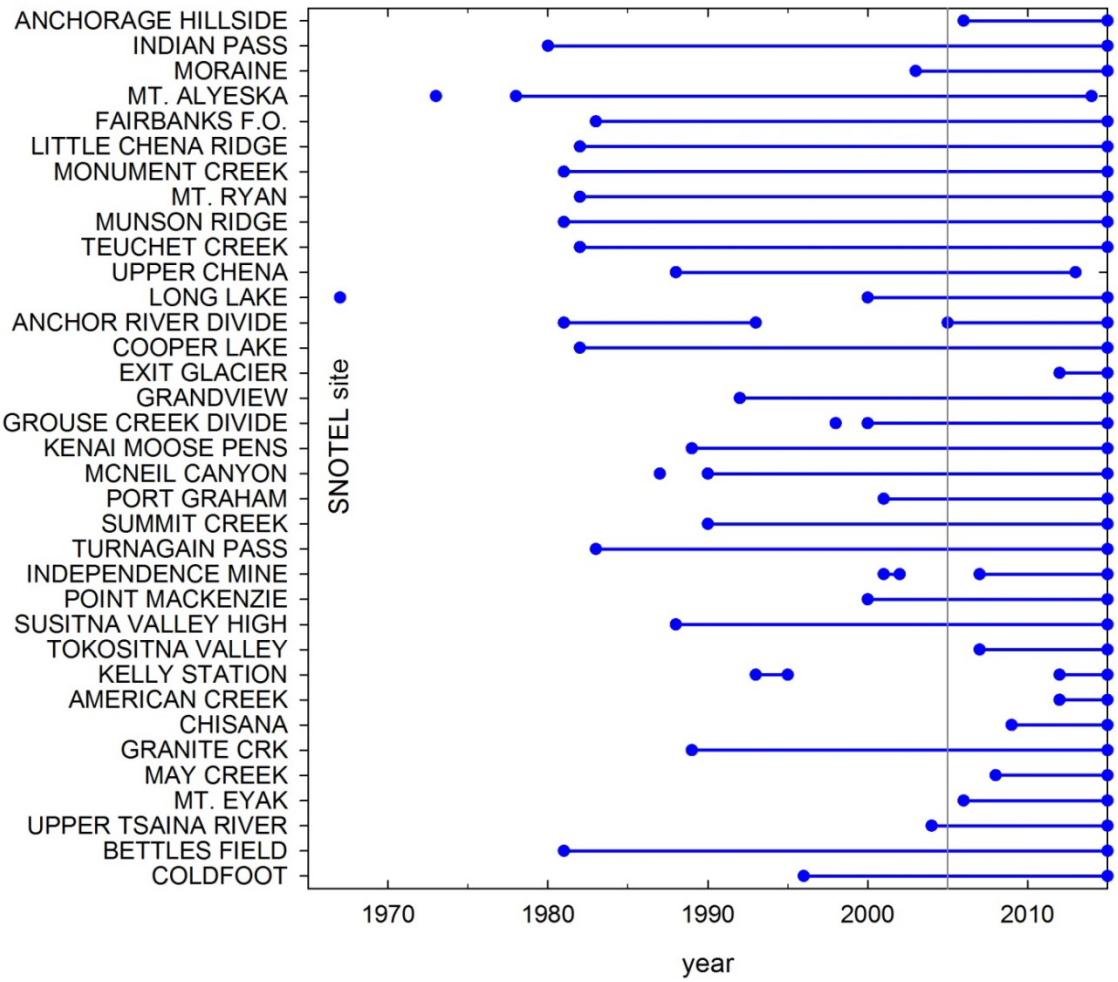

Figure 7. Period of record for the Alaska SNOTEL sites with SWE data. The beginning of the marked decline in the minimum Arctic sea ice extent in 2005 is shown by the *vertical gray line*. We are assuming that the AA effect begins then.

National Weather Service

We acquired daily SWE and snow depth data for the 22 NWS stations in Alaska where those data are reported. These airport sites are listed alphabetically in Table 2, showing the call letters, Cooperative Observer Program (COOP) ID, GHCND ID, location, elevation, and POR. The POR for the data we used are shown in Figure 8 for both the COOP (TD3200) data through 1996 and the GHCND data through June 2015 for the eight stations where we acquired that data. The beginning of the marked decline in the minimum Arctic sea ice extent in 2005 is shown by the vertical gray line.

Table 2. National Weather Service stations in Alaska reporting daily SWE

Station	ID	COOP ID	GHCND ID	Latitude	Longitude	Elev. (m)	POR
ANCHORAGE	ACG	500280	USW00026451	61.167	−149.983	34	1953–1999, 2002
ANNETTE	ANN	500352		55.033	−131.567	34	1982–1996
BARROW	BRW	500546		71.300	−156.783	9	1971–1996
BARTER IS	BTI	500558		70.133	−143.600	12	1971–1988
BETHEL	BET	500754		60.783	−161.717	5	1964–1980
COLD BAY	CDB	502102		55.200	−162.717	30	1971–1996
CORDOVA	CDV	502177		60.500	−145.500	13	1964
FAIRBANKS	FAI	502968	USW00026411, USC00502965	64.817	−147.867	133	1953–2001, 2011–2015
HOMER	HOM	503665		59.633	−151.500	27	1983–1996
JUNEAU	JNU	504100	USW00025309	58.367	−134.583	4	1953–1979, 1999–2001
KING SALMON	AKN	504766		58.683	−156.650	15	1971–1977
KODIAK	ADQ	504988		57.750	−152.500	5	1975–1976
KOTZEBUE	OTZ	505076		66.867	−162.633	3	1968–1996
MCGRATH	MCG	505769	USW00026510	62.967	−155.617	105	1955–2005
NOME	OME	506496		64.500	−165.433	4	1971–1996
SHEMYA	SYA	508118		57.150	−170.217	9	1984–1996
ST PAUL ISLAND	SNP	508419		52.717	174.100	37	1964–1965
SUMMIT	UMM	508811	USW00026414	63.333	−149.133	734	1971–1976
TALKEETNA	TKA	508976	USW00026528	62.300	−150.100	105	1970–1990, 1996–1998
UNALAKLEET	UNK	509564		63.883	−160.800	5	1974–1996
VALDEZ	VDZ	509686	USW00026442	61.133	−146.350	7	1976–2005
YAKUTAT	YAK	509941	USW00025339	59.517	−139.667	9	1953–2004

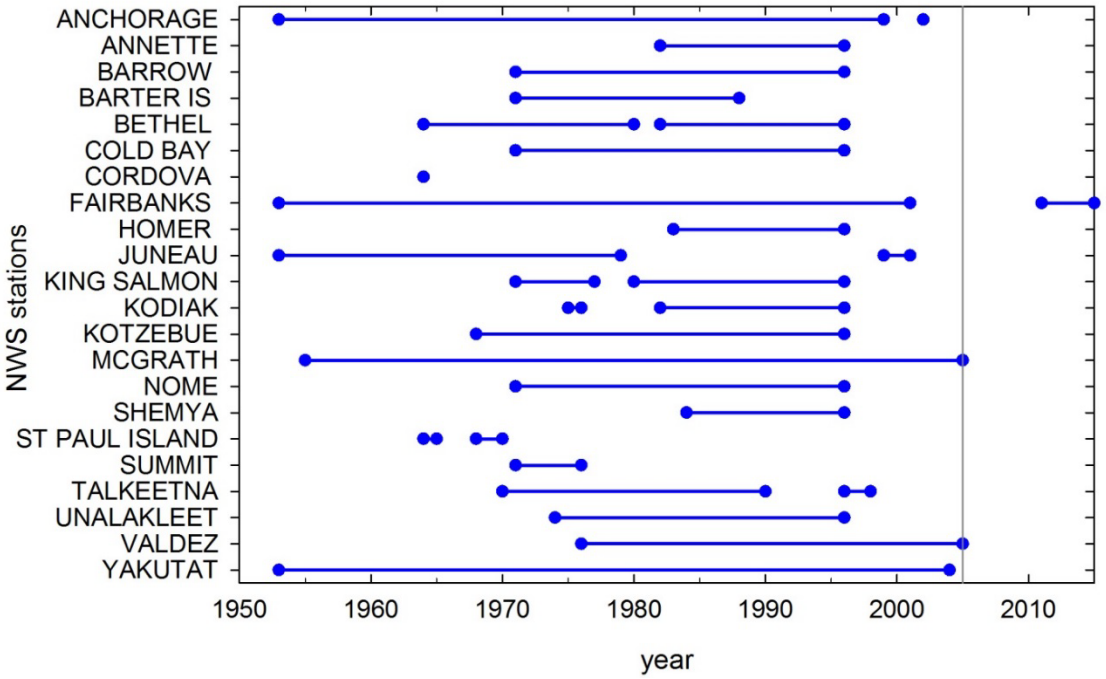

Figure 8. Periods of record for the Alaska NWS stations with SWE data. The beginning of the marked decline in the minimum Arctic sea ice extent in 2005 is shown by the *vertical gray line*.

Our initial inspection of the NWS COOP data indicated that most of the SWE values at most of the NWS stations were determined by dividing the snow depth by 10. Figure 9 shows depth-to-SWE ratios for Barrow and Fairbanks. The dark gray bar shows the number of ratios between 9.01 and 10.0 while the light gray bars show the distribution of depth-to-SWE ratios when ratios of exactly 10 are removed. At Barrow, it appears that SWE was typically estimated by dividing the measured depth by 10 while at Fairbanks SWE was often measured rather than estimated. This 10:1 rule may not be unreasonable for recently fallen snow at some temperatures but is likely to significantly underestimate SWE in a snowpack late in the accumulation season when the maximum SWE occurs. Appendix A shows histograms of the depth-to-SWE ratio from COOP data for all 22 NWS stations in Alaska.

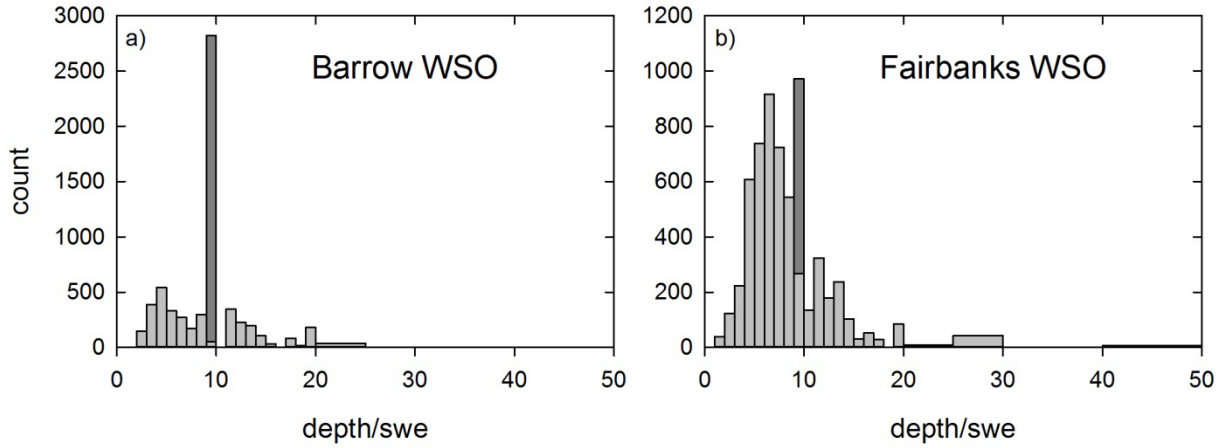

Figure 9. Snow-depth-to-SWE ratios for (*a*) Barrow and (*b*) Fairbanks from COOP data. The *dark gray bar* shows the ratio prior to the removal of data with ratio of exactly 10.

We obtained additional depth and SWE data from the GHCND archive for the eight NWS stations where it appears that SWE was typically measured rather than estimated. The GHCND data extend the POR back to the mid-1950s for five of the stations and to 2005 for two of the stations. Only Fairbanks has data from 2005 on, representing the climate associated with AA. Measurements were made at one Fairbanks location through 2001 and then began again at a different location, but still at the Fairbanks Airport, in 2011 and have continued to the present.

We processed the GHCND data to replace SWE values with 99 indicating *unknown* on days when the ratio was exactly 10. We manually corrected obvious errors where, for example, the depth or SWE suddenly changed by a factor of 10 while the other value remained the same. We also further refined our unknowns. If snow depth increased from one day to the next, we assume that it snowed (or rained) and that SWE increased. So on days with a larger snow depth than the previous day and SWE set to 99, we indicate unknown but increasing SWE by changing the unknown SWE to 90. Days with decreasing snow depth provide no information about SWE. That might indicate melting and a decrease in SWE or just consolidation of the snowpack and no change in SWE. Similarly, no change in snow depth does not provide information about ΔSWE. That might indicate no change in SWE but may also occur with rain and increasing SWE in the snowpack.

The histograms of the depth-to-SWE ratio in Figure 9 do not tell us when observers estimated SWE from the snow depth rather than measuring it. Estimating snow depths may have been limited to certain years. Figure 10 shows the number of days in the accumulation season, the number of those days with snowfall (ΔSWE > 0), the number with unknown but increasing SWE (ΔSWE = 90), and the number of those days with unknown SWE (ΔSWE = 99) for each year in the POR for the NWS stations at Anchorage and Valdez. The proportion of unknowns varies from year to year, but there is no obvious change in practice during either POR. Days with estimated rather than measured SWE occur throughout the POR at both stations but less frequently at Valdez than at Anchorage.

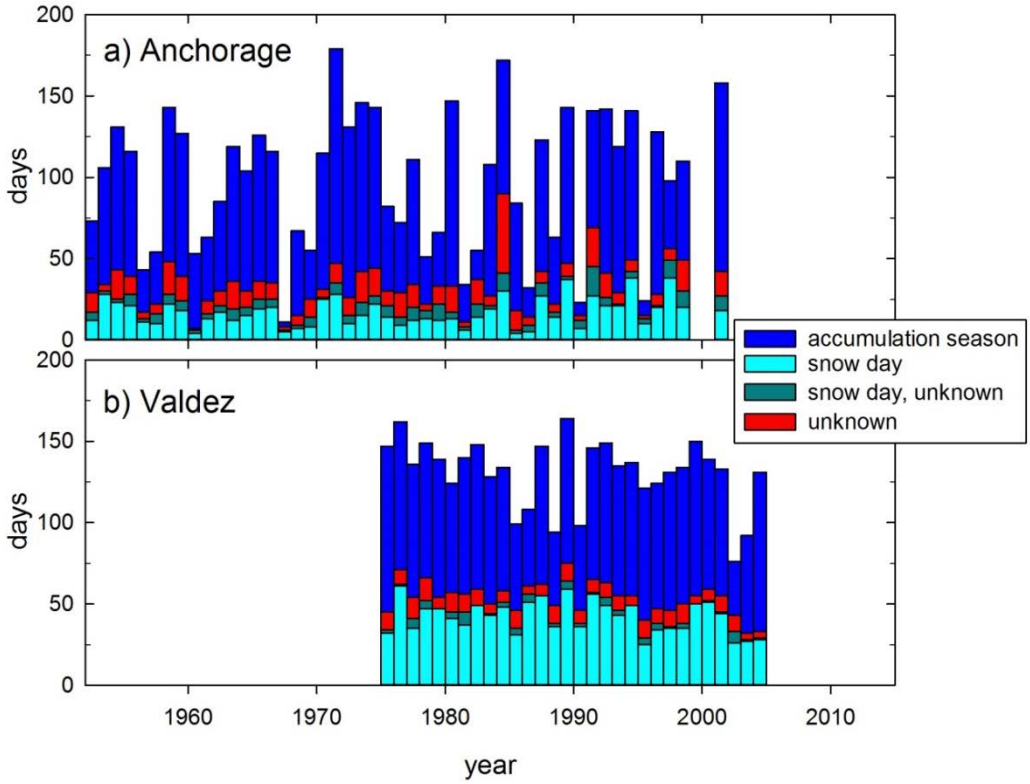

Figure 10. Period of record of SWE data at (*a*) Anchorage and (*b*) Valdez, showing the duration of the accumulation season with the number of snow days, the number of days with snow but with an unknown amount, and the number of days with no SWE information superposed.

Table 3 summarizes the information on unknown ΔSWE for the whole POR for all eight stations where SWE was frequently measured. On average, snowfall occurs on 17% of the days in the accumulation season in Anchorage; and on 16% of days, ΔSWE from the previous day is not known. SWE was measured more frequently in Valdez compared to the other NWS stations. On average, snowfall occurs on 32% of the days in the accumulation season in Valdez; and on 9% of days, the change in SWE from the previous day is not known. These ratios indicate that the SWE dataset for the NWS stations is missing significant information for characterizing the accumulation season climate and for generating synthetic SWE. Furthermore, only one of these eight stations with relatively frequent SWE measurements has data during the years characterized by AA. Therefore, we did not use the NWS data for generating synthetic SWE.

However, we obtained NARR and PASR data at grid points near the NWS stations to characterize the accumulation season.

Table 3. Fraction of days with specified positive ΔSWE (snow days) and days with unknown ΔSWE > 0 or unknown ΔSWE during the accumulation season.

	Snow days fraction	Unknown days fraction
Anchorage	0.17	0.16
Fairbanks	0.18	0.11
Juneau	0.22	0.22
McGrath	0.17	0.12
Summit	0.24	0.16
Talkeetna	0.19	0.16
Valdez	0.32	0.09
Yakutat	0.29	0.16

North American Regional Reanalysis

We extracted SWE for the NARR grid points representing the SNOTEL, NWS, and military locations. For some locations, the closest NARR grid point is in the ocean, where SWE data is not provided, so the nearest land grid point is used. Table 4 lists the NARR points by county and by grid point (NARR i and NARR j) order within the county along with the corresponding SNOTEL, NWS, or military site name. Ten of the NARR grid points correspond to more than one SNOTEL or NWS location. In those cases, the NARR information in the table is left blank for the additional locations. Time series of a few years of NARR SWE along with data from the associated NWS and SNOTEL sites are shown in Figure 11 for the NARR grid point closest to the Fairbanks SNOTEL and NWS locations (mapped in Figure 12) and for a grid point on the Kenai Peninsula closest to NWS station Homer and SNOTEL sites Anchor River Divide and McNeil Canyon. Both the NARR and NWS data tend to be noisy compared to the SNOTEL data, with large positive and negative daily increments in SWE.

We calculated the same statistics for the NARR data as we had for the SNOTEL data. We expand on the parameter values characterizing the accumulation season at each location by identifying other locations where that parameter has a similar distribution. For parameters with values that are binned, we use the chi-square test to compare data samples. For parameters with continuous values, we use the Kolmogorov-Smirnov test. As for the SNOTEL data, we created synthetic NARR data by using the characteristics of the pre-AA and AA eras.

Table 4. NARR gridded data acquired for SNOTEL, NWS, and military locations.

Site	Type	County	Latitude	Longitude	NARR i	NARR j	NARR lat	NARR lon
COLD BAY	NWS	Aleutians E	55.20	−162.72	76	200	55.44	−162.39
INDIAN PASS	SNOTEL	Anchorage	61.07	−149.48	106	201	60.97	−149.67
ANCHORAGE HIL	SNOTEL	Anchorage	61.11	−149.67				
ELMENDORF AFB	Military	Anchorage	61.26	−149.80	106	202	61.21	−149.99
ANCHORAGE	NWS	Anchorage	61.17	−149.98				
MT. ALYESKA	SNOTEL	Anchorage	60.96	−149.09	107	200	60.88	−148.86
FT RICHARDSON	Military	Anchorage	61.23	−149.62	107	202	61.36	−149.49
MORAINE	SNOTEL	Anchorage	61.38	−149.00	108	202	61.52	−148.99
BETHEL	NWS	Bethel	60.78	−161.72	89	213	60.75	−161.91
MCGRATH	NWS	Bethel	62.97	−155.62	102	212	62.89	−155.47
SUMMIT	NWS	Denali	63.33	−149.13	111	208	63.42	−149.40
CLEAR AS	Military	Denali	64.75	−148.86	114	212	64.82	−149.15
EIELSON AFB	Military	Fairbanks NS	64.70	−147.07	116	210	64.64	−147.34
FAIRBANKS F.O.	SNOTEL	Fairbanks NS	64.85	−147.80	116	211	64.88	−147.67
FT WAINWRIGHT	Military	Fairbanks NS	64.83	−147.62				
FAIRBANKS	NWS	Fairbanks NS	64.82	−147.87				
MUNSON RIDGE	SNOTEL	Fairbanks NS	64.85	−146.21	118	210	64.92	−146.20
LITTLE CHENA RI	SNOTEL	Fairbanks NS	65.12	−146.73	118	211	65.16	−146.53
MONUMENT CRK	SNOTEL	Fairbanks NS	65.08	−145.87	119	210	65.06	−145.62
TEUCHET CREEK	SNOTEL	Fairbanks NS	64.95	−145.52				
MT. RYAN	SNOTEL	Fairbanks NS	65.25	−146.15	119	211	65.30	−145.95
UPPER CHENA	SNOTEL	Fairbanks NS	65.10	−144.93	120	210	65.20	−145.04
JUNEAU	NWS	Juneau	58.37	−134.58	125	181	58.32	−134.85
JUNEAU2					126	181	58.42	−134.34
LONG LAKE	SNOTEL	Juneau	58.19	−133.83	127	180	58.25	−133.63
PORT GRAHAM	SNOTEL	Kenai Pen	59.35	−151.85	100	198	59.30	−151.60
HOMER	NWS	Kenai Pen	59.63	−151.50	101	199	59.54	−151.92
MCNEIL CANYON	SNOTEL	Kenai Pen	59.74	−151.25				
ANCHOR RIV DIV	SNOTEL	Kenai Pen	59.86	−151.32				
ANCHOR RIV DI2					102	199	59.86	−150.98
KENAI MOOSE PE	SNOTEL	Kenai Pen	60.73	−150.48	104	201	60.66	−150.65
COOPER LAKE	SNOTEL	Kenai Pen	60.39	−149.69	105	199	60.33	−149.53
GROUSE CRK DIV	SNOTEL	Kenai Pen	60.26	−149.34				
EXIT GLACIER	SNOTEL	Kenai Pen	60.19	−149.62				
GRANDVIEW	SNOTEL	Kenai Pen	60.61	−149.06	106	199	60.49	−149.04
TURNAGAIN PASS	SNOTEL	Kenai Pen	60.78	−149.18	106	200	60.73	−149.35
SUMMIT CREEK	SNOTEL	Kenai Pen	60.62	−149.53				
KODIAK	NWS	Kodiak Island	57.75	−152.50	96	194	57.70	−152.18
KODIAK2					96	195	57.94	−152.49
KING SALMON	NWS	Lake and Pen	58.68	−156.65	91	201	58.47	−156.65
KING SALMON2					92	202	58.65	−156.21
PT MACKENZIE	SNOTEL	Matanuska-Su	61.39	−150.03	106	203	61.45	−150.32
INDEPENDENCE	SNOTEL	Matanuska-Su	61.79	−149.28	108	203	61.76	−149.31
SUSITNA VALLEY	SNOTEL	Matanuska-Su	62.13	−150.04	108	205	62.24	−149.96
TALKEETNA	NWS	Matanuska-Su	62.30	−150.10				
TOKOSITNA VAL	SNOTEL	Matanuska-Su	62.63	−150.78	108	207	62.71	−150.63
NOME	NWS	Nome	64.50	−165.43	94	226	64.41	−165.16

Site	Type	County	Latitude	Longitude	NARR i	NARR j	NARR lat	NARR lon
UNALAKLEET	NWS	Nome	63.88	−160.80	98	220	63.93	−160.63
BARROW	NWS	North Slope	71.30	−156.78	119	236	71.02	−156.24
BARTER ISLAND	NWS	North Slope	70.13	−143.60	130	224	69.91	−143.53
KOTZEBUE	NWS	NW Arctic	66.87	−162.63	103	230	66.95	−162.61
KELLY STATION	SNOTEL	NW Arctic	67.93	−162.28	106	232	67.92	−161.98
GRANITE CREEK	SNOTEL	SE Fairbanks	63.94	−145.40	117	206	63.80	−145.47
FORT GREELY	Military	SE Fairbanks	63.91	−145.55				
CHISANA	SNOTEL	SE Fairbanks	62.07	−142.05	119	198	62.07	−142.02
AMERICAN CRK	SNOTEL	SE Fairbanks	64.79	−141.23	124	206	64.73	−141.46
MT. EYAK	SNOTEL	Valdez-Cord	60.55	−145.75	111	196	60.48	−145.65
CORDOVA	NWS	Valdez-Cord	60.50	−145.50				
VALDEZ	NWS	Valdez-Cord	61.13	−146.35	111	199	61.23	−146.53
UPPER TSAINA R	SNOTEL	Valdez-Cord	61.19	−145.65	112	198	61.12	−145.72
MAY CREEK	SNOTEL	Valdez-Cord	61.35	−142.71	117	196	61.30	−142.54
YAKUTAT3	NWS	Yakutat	59.52	−139.67	120	187	59.35	−138.71
YAKUTAT2					120	188	59.61	−138.95
GALENA AFB	Military	Yukon-Koy	64.75	−156.84	104	218	64.58	−156.80
GALENA AFB2					104	219	64.80	−157.21
BETTLES FIELD	SNOTEL	Yukon- Koy	66.92	−151.53	115	220	66.84	−151.56
COLDFOOT	SNOTEL	Yukon- Koy	67.25	−150.18	117	220	67.15	−150.38

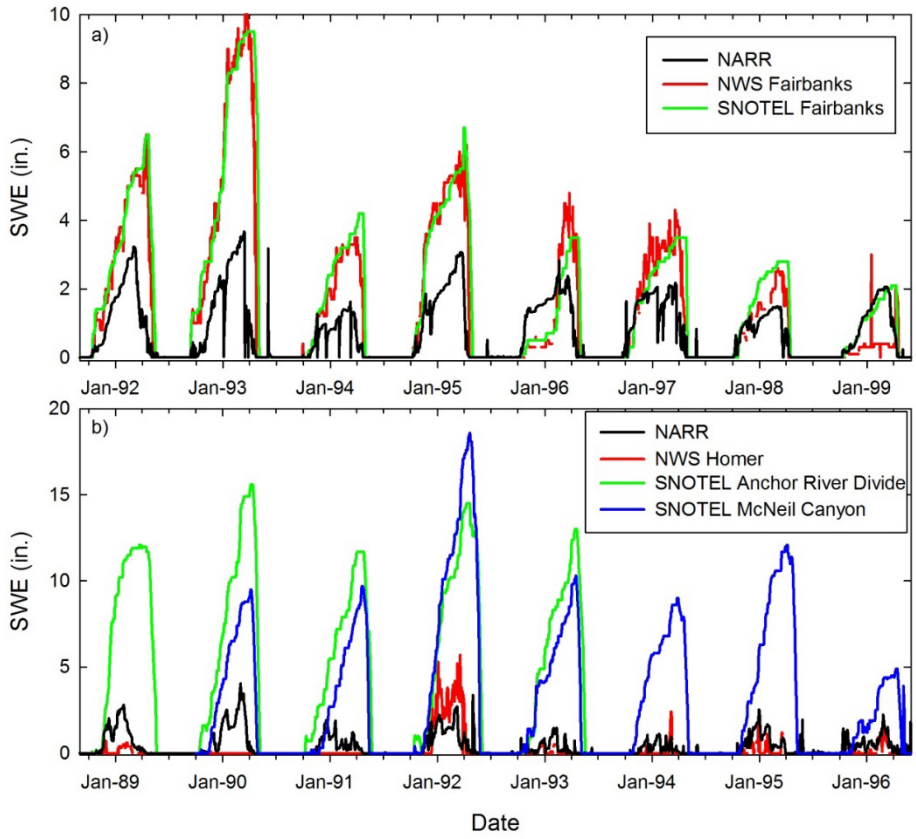

Figure 11. Time series comparisons for NARR grid points with associated NWS and SNOTEL sites for (*a*) two sites in the Fairbanks area and (*b*) three sites on the Kenai Peninsula.

Figure 12. NARR grid point near Fairbanks representing a SNOTEL site (Fairbanks F.O.), an NWS station (Fairbanks WSO), and Fort Wainwright. The time series of SWE for accumulations seasons from 1992 through 1999 are shown in Fig. 11.

Pan-Arctic Snow Reanalysis

We extracted PASR SWE for grid points representing the SNOTEL, NWS, and military locations. For some locations, the closest PASR grid point is in the ocean, where SWE data is not provided, so the nearest land grid point is used. Shemya is south of the PASR grid, and there are no grid points on land for Annette. For Yakutat, two PASR points at similar distances from the Yakutat NWS stations are both used. The 63 PASR points, named by the corresponding SNOTEL, NWS, or military site, are listed in Table 5 by county and by grid point order within the county. The table also includes the elevation and land-cover code for the grid point. Descriptions of the land-cover codes are provided in Table 6 (after Liston and Elder 2006a) along with the snow-holding depth and the leaf area index (LAI), which is used in SnowModel to determine the fraction of the falling snow that is intercepted by the tree canopy.

How does the PASR-modeled SWE during the accumulation season on a 10 km grid compare with SWE measurements at a point within the grid cell? Time series for the POR of PASR and SNOTEL SWE for four grid points where the SNOTEL site elevation is within 50 m of the grid-cell average elevation are shown in Figure 13. The region represented by the grid point in Figure 13a is characterized by upland shrubs, and the other three are characterized by coniferous forests. Photos of the four SNOTEL sites are provided in Figure 14. The SNOTEL and PASR SWE in both Figure 13a and b are similar. The significantly smaller PASR SWE compared to the SNOTEL values in Figure 13c and d may be due in part to a greater interception of snowfall by the tree canopy characterized by an LAI of 2.5 in the modeled snow events for these grid cells than occurs at the SNOTEL sites.

Table 5. PASR grid points. The last two columns show the elevation and land cover associated with that grid point. Land-cover code descriptions are provided in Table 6.

Name	County	PASR i	PASR j	PASR latitude	PASR longitude	Land cover	Elev. (m)
COLD BAY	Aleutians East	476	1	55.317	−162.615	6	8
ST PAUL ISLAND	Aleutians West	423	9	57.218	−170.317	19	7
ANCHORAGE	Anchorage	521	89	61.196	−149.997	14	17
ELMENDORF AFB	Anchorage	522	90	61.23	−149.749	6	203
ANCHORAGE HSIDE	Anchorage	523	89	61.103	−149.685	10	515
FORT RICHARDSON	Anchorage	523	90	61.183	−149.593	14	592
INDIAN PASS	Anchorage	524	89	61.056	−149.529	14	790
MORAINE	Anchorage	525	94	61.407	−148.911	14	796
MT. ALYESKA	Anchorage	526	89	60.961	−149.22	11	401
BETHEL	Bethel	463	58	60.766	−161.791	6	11
MCGRATH	Bethel	485	92	62.968	−155.715	6	135
CLEAR AS	Denali	507	125	64.722	−148.789	1	173
SUMMIT	Denali	513	111	63.329	−149.203	6	882
FAIRBANKS	Fairbanks NStar	510	128	64.812	−147.939	14	203
FAIRBANKS F.O.	Fairbanks NStar	510	129	64.89	−147.829	3	214
FORT WAINWRIGHT	Fairbanks NStar	511	129	64.841	−147.654	21	152
LITTLE CHENA RIDGE	Fairbanks NStar	513	134	65.128	−146.743	6	578
EIELSON AFB	Fairbanks NStar	514	129	64.692	−147.134	1	170
MT. RYAN	Fairbanks NStar	515	137	65.256	−146.047	6	724
MUNSON RIDGE	Fairbanks NStar	517	133	64.848	−146.166	6	531
MONUMENT CREEK	Fairbanks NStar	517	136	65.077	−145.818	14	743
TEUCHET CREEK	Fairbanks NStar	519	136	64.973	−145.474	15	709
UPPER CHENA	Fairbanks NStar	520	139	65.147	−144.947	14	943
JUNEAU	Juneau	610	120	58.38	−134.531	1	412
LONG LAKE	Juneau	614	122	58.243	−133.836	14	767
PORT GRAHAM	Kenai Peninsula	521	66	59.325	−151.952	1	109
KENAI MOOSE PENS	Kenai Peninsula	521	83	60.712	−150.53	1	74
HOMER	Kenai Peninsula	522	70	59.609	−151.478	24	56
MCNEIL CANYON	Kenai Peninsula	522	72	59.772	−151.314	11	294
ANCHOR RIV DIV	Kenai Peninsula	522	73	59.854	−151.23	6	440
SUMMIT CREEK	Kenai Peninsula	526	85	60.641	−149.583	14	972
COOPER LAKE	Kenai Peninsula	527	82	60.354	−149.699	1	600
TURNAGAIN PASS	Kenai Peninsula	527	87	60.754	−149.249	3	642
EXIT GLACIER	Kenai Peninsula	528	81	60.226	−149.636	1	752
GROUSE CRK DIVIDE	Kenai Peninsula	529	82	60.259	−149.396	1	544
GRANDVIEW	Kenai Peninsula	529	86	60.579	−149.036	14	852
KODIAK	Kodiak Island	526	50	57.785	−152.456	11	121
KING SALMON	Lake and Peninsula	499	48	58.702	−156.605	14	29
TOKOSITNA VALLEY	Matanuska-Susitna	510	100	62.587	−150.761	10	658
TALKEETNA	Matanuska-Susitna	515	99	62.278	−150.033	1	176
SUSITNA VALLEY HI	Matanuska-Susitna	516	98	62.151	−149.965	1	201
POINT MACKENZIE	Matanuska-Susitna	520	91	61.403	−149.972	3	30
INDEPENDENCE MINE	Matanuska-Susitna	521	96	61.757	−149.352	14	839
NOME	Nome	433	92	64.481	−165.496	15	85
UNALAKLEET	Nome	457	92	63.927	−160.81	6	62

Name	County	PASR i	PASR j	PASR latitude	PASR longitude	Land cover	Elev. (m)
BARROW2	North Slope	445	173	71.287	−156.838	17	7
BARTER IS2	North Slope	493	186	70.165	−143.52	14	8
KELLY STATION	NW Arctic	437	131	67.912	−162.234	14	99
KOTZEBUE	NW Arctic	439	120	66.895	−162.56	14	3
FORT GREELY	SE Fairbanks	525	126	63.9	−145.618	1	497
GRANITE CRK	SE Fairbanks	526	127	63.923	−145.341	1	382
AMERICAN CREEK	SE Fairbanks	537	147	64.794	−141.129	1	483
CHISANA	SE Fairbanks	552	121	62.051	−141.993	6	1308
VALDEZ	Valdez-Cordova	538	99	61.103	−146.284	14	573
UPPER TSAINA RIV	Valdez-Cordova	541	102	61.23	−145.681	14	1209
MT. EYAK	Valdez-Cordova	545	96	60.56	−145.695	18	223
CORDOVA	Valdez-Cordova	546	96	60.507	−145.55	1	114
MAY CREEK	Valdez-Cordova	554	113	61.35	−142.602	3	847
YAKUTAT	Yakutat	579	108	59.529	−139.722	1	6
YAKUTAT2	Yakutat	580	108	59.529	−139.722	15	5
GALENA AFB	Yukon-Koyukuk	472	107	64.718	−156.883	6	44
BETTLES FIELD	Yukon-Koyukuk	484	139	66.891	−151.577	1	201
COLDFOOT	Yukon-Koyukuk	487	145	67.239	−150.325	6	572

Table 6. Land-cover categories for PASR data.

Table	Description	Snow-holding depth (m)	Leaf Area Index summer/winter
1	Coniferous forest	15	2.5/2.5
2	Deciduous forest	12	2.5/0.5
3	Mixed forest	14	2.5/1.5
4	Scattered short-conifer	8	1.5/1.5
5	Clearcut conifer	4	1.0/1.0
6	Mesic upland shrub	0.5	—
7	Xeric upland shrub	0.25	—
8	Playa shrubland	1	—
9	Shrub wetland/riparian	1.75	—
10	Erect shrub tundra	0.65	—
11	Low shrub tundra	0.3	—
12	Grassland rangeland	0.15	—
13	Subalpine meadow	0.25	—
14	Tundra (non-tussock)	0.15	—
15	Tundra (tussock)	0.2	—
16	Prostrate shrub tundra	0.1	—
17	Arctic gram, wetland	0.2	—
18	Bare	0.01	—
19	Water/possibly frozen	0.01	—
20	Permanent snow/glacier	0.01	—
21	Residential/urban	0.01	—
22	Tall crops	0.4	—
23	Short crops	0.25	—
24	Ocean	—	—

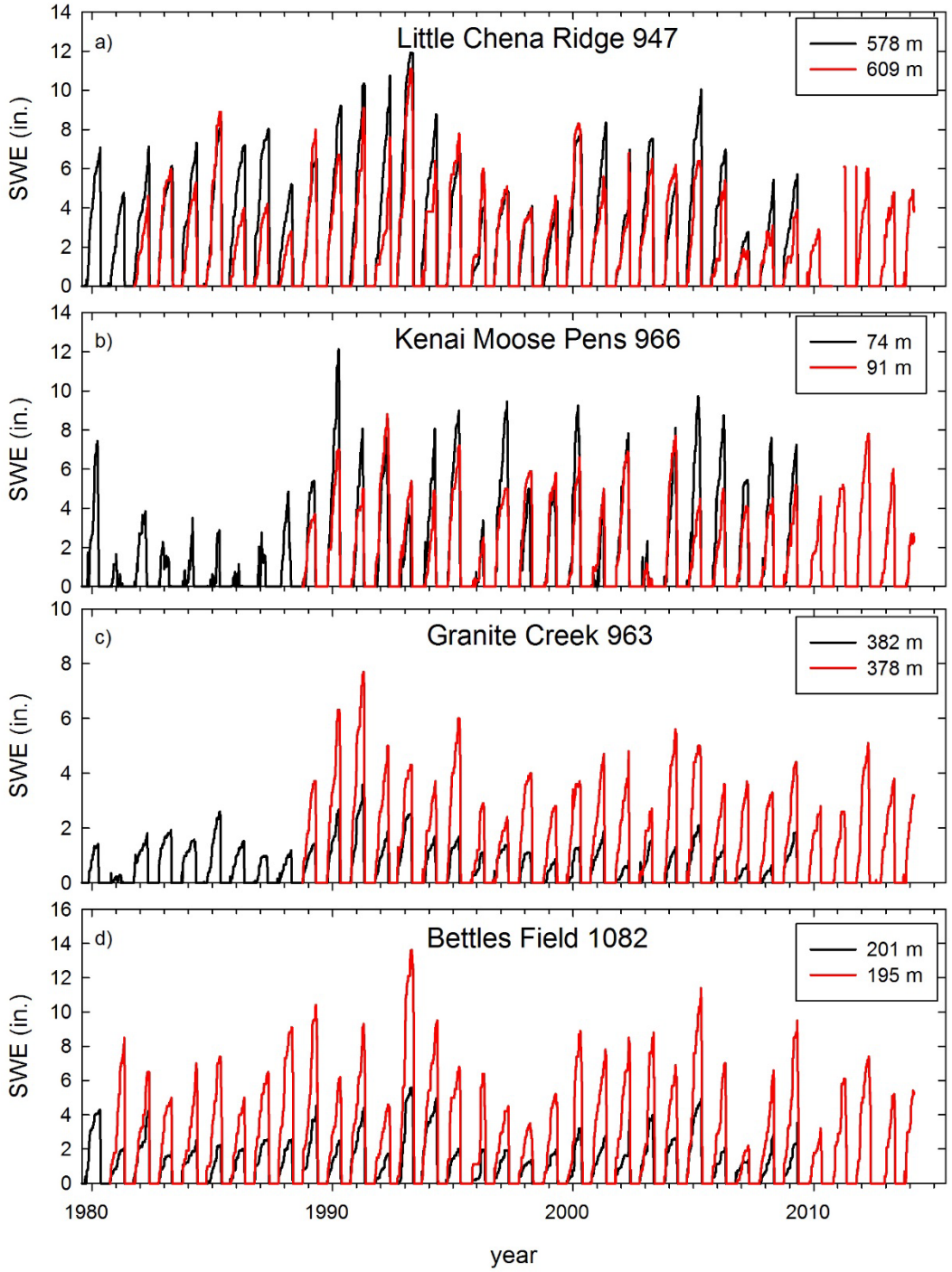

Figure 13. PASR (*black line*) and SNOTEL (*red line*) SWE for four locations where the SNOTEL elevation is within 50 m of the PASR grid point elevation and the SNOTEL POR is relatively long. The grid point in (*a*) is characterized by mesic upland shrubs, and the rest are coniferous forests. Photos of the SNOTEL sites are in Fig. 14.

a)  b) 

c)  d) 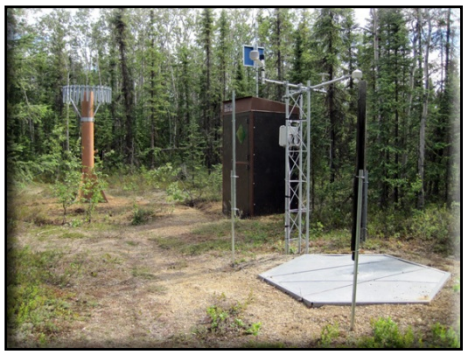

Figure 14. Photos of the SNOTEL sites in Fig. 13.

We calculated the same statistics for the PASR data as for the SNOTEL and NARR data. We expand on the parameter values characterizing the accumulation season at each location by identifying other locations where that parameter has a similar distribution. For parameters with values that are binned, we use the chi-square test to compare data samples. For parameters with continuous values, we use the Kolmogorov-Smirnov test. Using the characteristics of the accumulation season in the pre-AA and AA eras, we created synthetic PASR data.

Synthetic Data

We generated synthetic SWE data with characteristics consistent with the measured SNOTEL, NARR, or PASR data for the accumulation season. We used two parameters that are correlated with the maximum SWE in each winter to characterize the accumulation seasons at each site: the number of days with snowfall and the 80th% ΔSWE. Because there are relatively few winters at each site in each of the eras, we expanded the choices of parameter values for the site by including sites that are similar. For a winter of synthetic SWE for each location (SNOTEL site or NARR or PASR grid point), we randomly chose values for the two parameters from the expanded distributions of those values for that location. Then, for each day in what will become the accumulation season, we randomly chose the value of ΔSWE from the expanded ΔSWE distribution for the location, allowing for negative, zero, and positive daily ΔSWE. Each day with $\Delta SWE > 0$ uses one of the allotted days with snowfall. The accumulation season ends on the last day with snowfall. If that results in the maximum SWE for the accumulation season, that

winter is complete. If, however, the actual maximum occurred earlier in the accumulation season, that synthetic winter is deleted and rebuilt from the beginning.

For each location, we generated 499 years of synthetic data consistent with the characteristics of the accumulation seasons pre-AA and 499 years of synthetic data consistent with the AA-era accumulation seasons.

Extreme Value Analysis

Our ultimate goal is to use the synthetic data to determine if extreme snow loads in the AA era with greater persistence in weather patterns are different from snow loads in the pre-AA era. In the EVA, we follow Hoskings and Wallis (1997), adapting the xsim.for Fortran program for this project. That program is provided by Hosking (2005). In the following, we briefly describe their regional frequency analysis approach.

First, the "regional" in the name refers to the combination of data from a variety of independent locations to provide a larger dataset for defining the extreme value distributions. This is done to reduce sampling error. The locations included in the dataset define the region, but the there is no requirement that the locations be contiguous. The data at each location are normalized by the location mean so that the shape of the fitted extreme value distributions is the same at all locations in a region, with the scale provided by the location mean. The regional frequency analysis approach includes tests for discordancy and heterogeneity so that the user is alerted to possible errors in the data at a location and any lack of homogeneity in the tentative region. Users can then readjust the region groupings to reduce heterogeneity. In our analysis, the POR of the synthetic data is long, so there is no need to group the locations into regions.

The Hosking and Wallis (1997) approach uses L-moments and L-moment ratios rather than conventional moments (mean, variance, skewness, and kurtosis) to characterize the data and to fit extreme value distributions. The *r*th L-moment is

$$\lambda_r = \int_0^1 x(u) P^*_{r-1}(u)\, du \qquad (1)$$

where λ_r is the quantile function for the random variable X and $P^*_{r-1}(u)$ is the shifted Legendre polynomial of order *r*. The first L-moment, λ_1, is the mean. The ratio of the first and second L-moments, $\tau = \lambda_2/\lambda_1$, is called the L-CV, analogous to the conventional coefficient of variation. The higher L-moment ratios are the L-skewness, $\tau = \lambda_3/\lambda_2$, and L-kurtosis, $\tau = \lambda_4/\lambda_2$.

Sample L-moments are calculated from a sample of data (e.g., annual extremes) of size *n* (number of years), arranged in ascending order by first calculating the sample probability weighted moments,

$$b_r = \frac{1}{n}\sum_{j=r+1}^{n}\frac{(j-1)(j-2)...(j-r)}{(n-1)(n-2)...(n-r)}x_{j:n}, \tag{2}$$

and then by calculating the sample L-moments from the b_r:

$$\begin{aligned} l_1 &= b_0 \\ l_2 &= 2b_1 - b_0 \\ l_3 &= 6b_2 - 6b_1 + b_0 \\ l_4 &= 20b_3 - 30b_2 + 12b_1 - b_0. \end{aligned} \tag{3}$$

The sample L-CV and L-moment ratios are

$$\begin{aligned} t &= \frac{l_2}{l_1} \\ t_3 &= \frac{l_3}{l_2} \\ t_4 &= \frac{l_4}{l_2}. \end{aligned} \tag{4}$$

In this application we calculated the sample L-moments from the ordered samples of the 499 synthetic years of annual maximum SWE. The L-moment ratios t_3 and t_4 for our synthetic SNOTEL, NARR, and PASR data for all the locations and both eras are plotted in Figure 15. In the L-skewness vs. L-kurtosis plane of this figure, 3-parameter distributions are curves. The five 3-parameter distributions plotted are the generalized logistic (GLO), generalized extreme value (GEV), lognormal (LN3), Pearson Type III (PE3), and generalized Pareto (GPA). For a given value of L-skewness, the L-kurtosis and the length of the tail of the distribution increases, going from the GPA distribution (or PE3 distribution at high L-skewness) to the GLO distribution. Two-parameter distributions, including the often-assumed Gumbel extreme value distribution, are points in the plane, labeled by the first letter in the name of the distribution. The 4-parameter kappa distribution fills most of the plane below the GLO curve. The GLO, GEV, LN3, and GPA density distributions for four values of L-skewness ranging from 0.05 to 0.35 are plotted in Figure 16. The tails of the distributions get longer (k decreases and becomes negative) as τ_3 increases because τ_4 is also increasing, following the curves in Figure 15. The L-skewness values for our synthetic data generally fall in the range of 0.05 to 0.35 and tend to cluster around the GEV, LN3, and PE3 curves. The means of the datasets, shown by triangles, indicate that the NARR data for both eras tend to have relatively high values of L-kurtosis and L-skewness and therefore longer tails than the other datasets. The PASR data for the AA era tends to (a) have low L-kurtosis and L-skewness and therefore relatively short tails and (b) fall between the GPA and GEV distributions. This diagram provides only an overview of the characteristics of the datasets. Determining the best distributions to use and the confidence interval around the distribution is done in the xsim.for Fortran program provided by Hosking (2005).

We adapted the Hosking xsim.for program to use the L-moments of the synthetic data for each location and era to fit a 4-parameter kappa distribution. The program then samples that distribution to simulate *N* years of data (*N* = 499 in this case) and fits the five 3-parameter distributions to those samples. This sampling is done a user-specified number of times (we specified 1000), and the best 3-parameter distribution and acceptable 3-parameter distributions are determined based on a goodness-of-fit test. Xsim.for is then rerun in a different mode to determine the confidence intervals around the best-fit curve for the user-specified choice of a kappa distribution or one of the 3-parameter distributions. The program samples the distribution to simulate *N* years of data and fits the specified distribution to that data for a number of repetitions chosen by the user (we specified 2000). These repetitions provide the 5% and 95% confidence intervals for the fitted distribution.

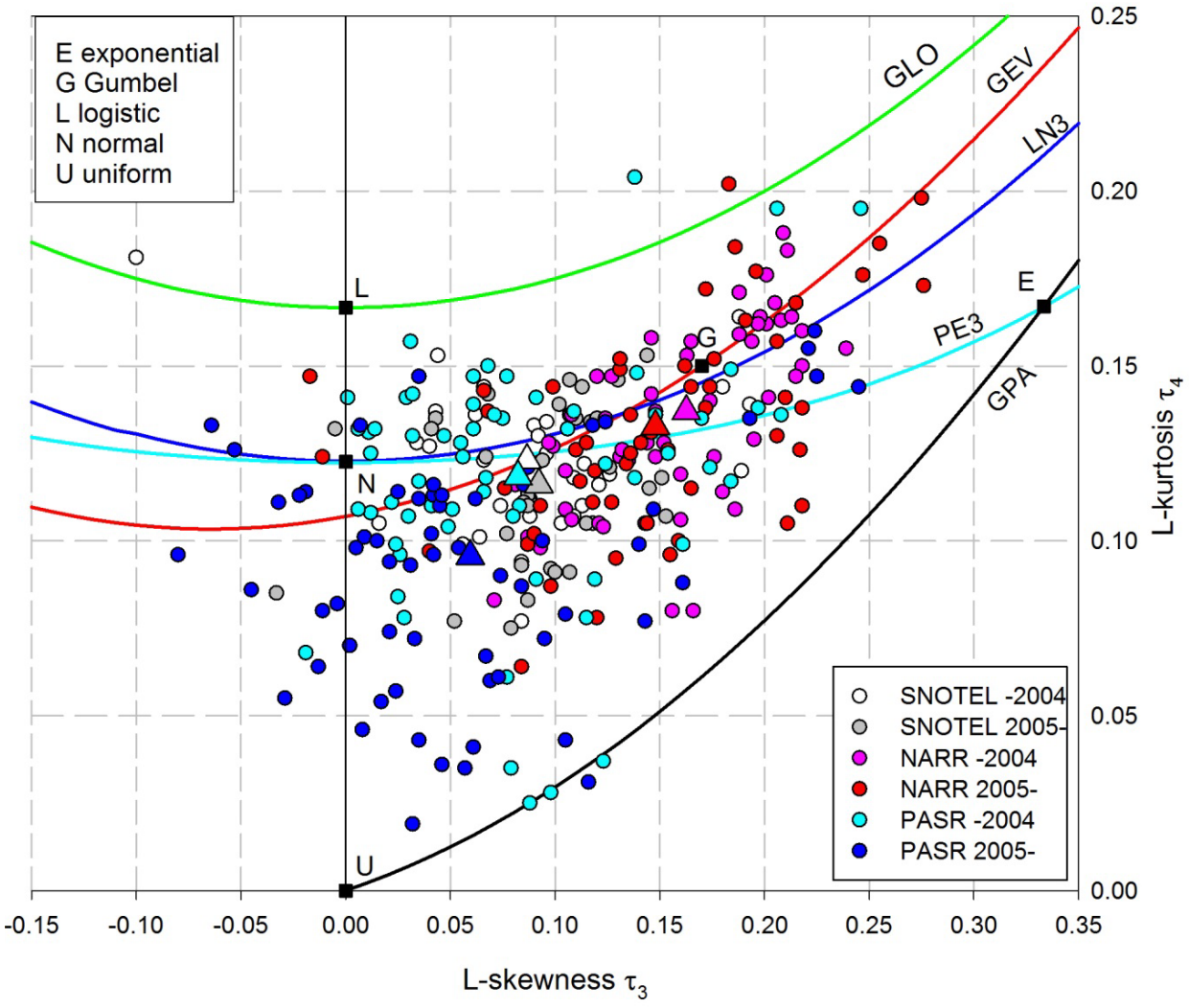

Figure 15. L-moment ratio diagram showing the relationships between the various 3-parameter and 2-parameter extreme value distributions and sample L-moment ratios for the two eras (through 2004 and 2005 and on) of the three sets of synthetic data. The means for the datasets are shown by *triangles*.

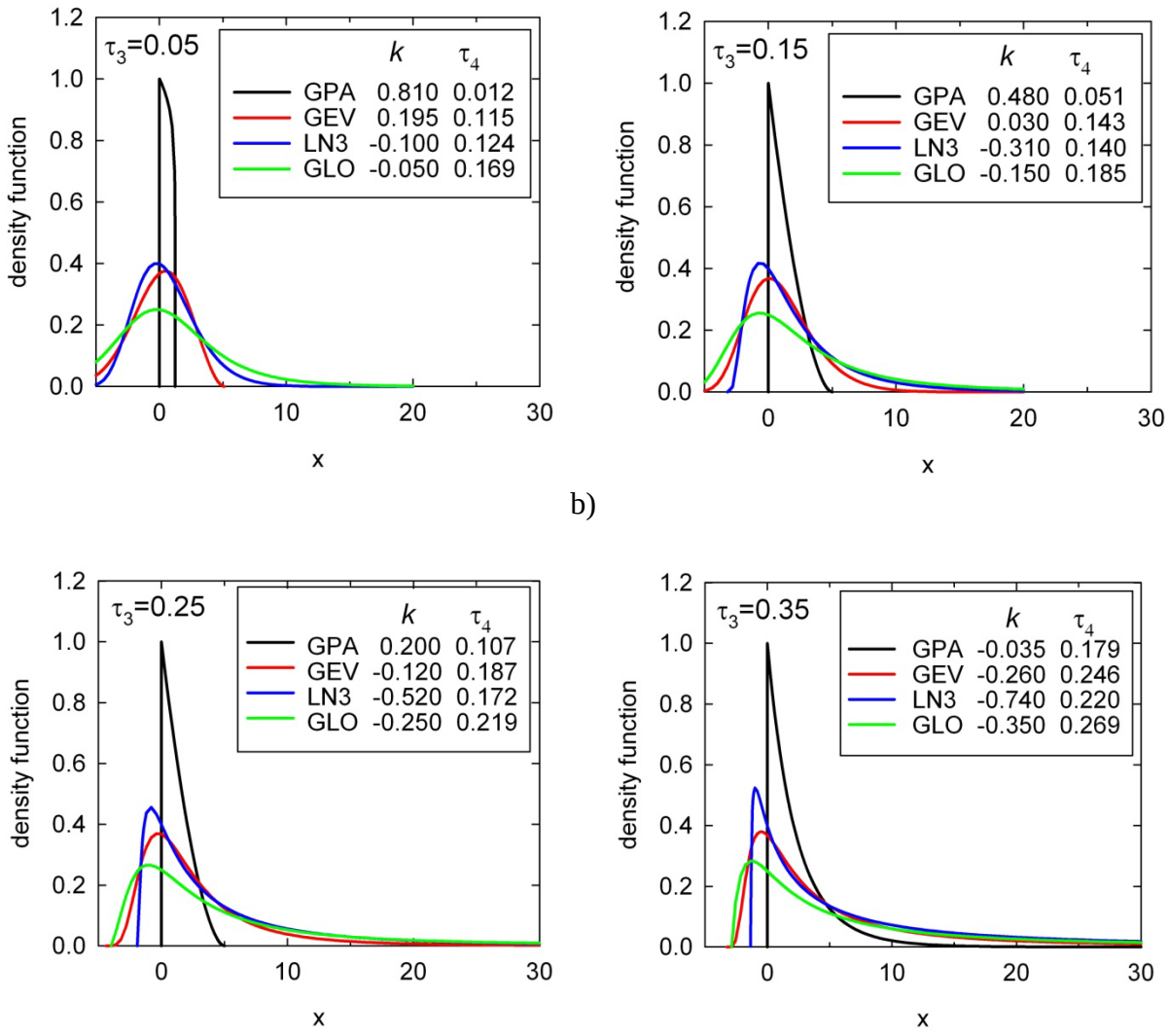

Figure 16. Extreme value distributions for increasing values of τ_3: (*a*) $\tau_3 = 0.05$, (*b*) $\tau_3 = 0.15$, (*c*) $\tau_3 = 0.25$, and (*d*) $\tau_3 = 0.35$. The tails of the distributions get longer as τ_3 increases because τ_4 is also increasing.

Global Climate Model Data

We did an EVA of the simulation of twenty-first century GCM SWE. Because the climate changes throughout the century, the GCM data is not stationary. We reduced this trend in time by using 33- or 34-year-long blocks (depending on the GCM POR) of annual maximum SWE in the EVA. We moved the block in 10-year increments; so the first block of data ends around 2039, and the final block ends in the last year of the simulation for that GCM. Like the synthetic SNOTEL, NARR, and PASR L-moments, the GCM L-moments tend to cluster around the GEV, LN3, and PE3 curves in the L-moment diagram. Therefore, we fit GEV and LN3 distributions to the blocks of GCM data.

Results and Discussion

SNOTEL Data

At most SNOTEL sites, the annual maximum SWE is significantly correlated with the number of days with snowfall and with the 80th% ΔSWE (Figure 17a). At 12 of the sites, the correlation between maximum SWE and the number of days with snowfall is significant, but the correlations with 80th% ΔSWE are not. Eight of those sites have relatively short POR (between 4 and 16 years), which may explain the low correlation and lack of significance. Not shown in Figure 17a is American Creek with only four years of data and a negative correlation between the maximum SWE and the number of days with snow. The correlation between maximum SWE and other parameters of the accumulation tends to be smaller than those shown in Figure 17a. The correlation of maximum SWE with the number of days in the accumulation season and the e^2-folding lag are shown in Figure 17b. The correlations at most sites are not significant; and maximum SWE often has a negative, but not significant, correlation with lag. Note that winters with long periods of no snow and a resulting small snow accumulation may be characterized by relatively large lags. The number of days with snowfall and the 80th% ΔSWE are relatively independent (Figure 18).

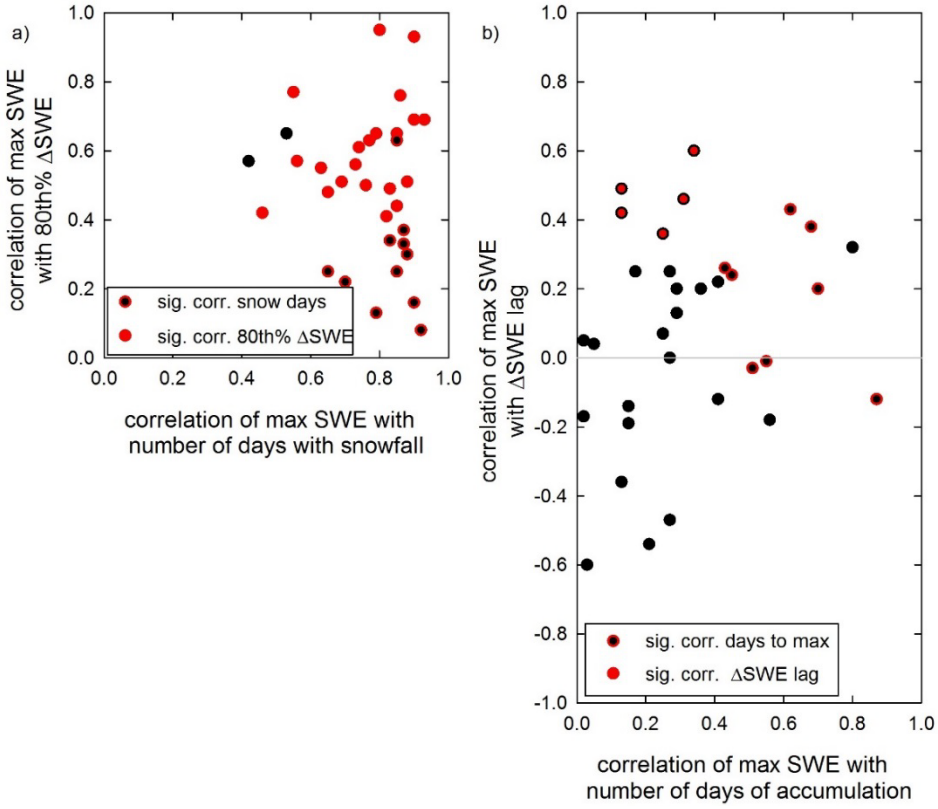

Figure 17. Correlations of the annual maximum SWE with parameters of the accumulation season at the SNOTEL sites: (*a*) max SWE and 80th% ΔSWE vs. max SWE and number of days with snowfall and (*b*) max SWE and e^{-2}-folding lag vs. max SWE and number of days in the accumulation season. Significant correlations are shown by a *red outline*, *red fill*, or *both*.

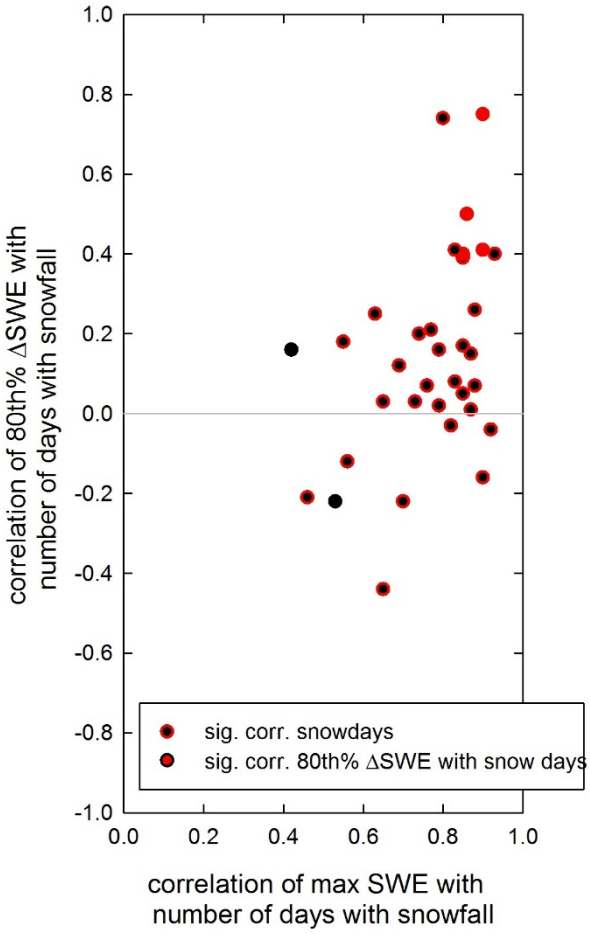

Figure 18. Correlation of the 80th% ΔSWE and the number of days with snowfall plotted vs. the correlation of max SWE and the number of days with snowfall. Significant correlations are shown by a *red outline*, *red fill*, or *both*.

Basic data comparing SNOTEL accumulation season parameters in the pre-AA and AA eras are shown in Figure 19. Figure 19a and b show the mean number of days in the accumulation season and the mean number of days with snowfall in the accumulation season. Figure 19c and d are the mean annual maximum SWE and the mean absolute deviation of the annual maximum SWE from the mean value. An increase in absolute deviation would indicate a greater variation in the snow load from year to year, a possible result of AA. The two final plots in Figure 19 deal with means of the daily conditions during the accumulation season. Figure 19e shows the mean 80th% daily ΔSWE on days with ΔSWE > 0, and Figure 19f shows the mean e^2-folding lag for daily ΔSWE. In all six plots, values that are significantly different (less than a 5% probability of being drawn from the same population) are in red. That occurs for five sites for the number of days with snowfall, three sites for the annual maximum SWE, and one site for 80th% ΔSWE. The sites with significantly different means have fewer snowfall days, a smaller annual maximum

SWE, and smaller 80th% ΔSWE in the AA era compared to pre-AA. The other characteristics of the accumulation season are not significantly different between the two periods at any of the sites. This general lack of differentiation between the two eras may be because AA has little effect on snow accumulation at these sites or just because of the relatively short records in the two eras.

Because of the generally significant correlation of the maximum SWE with the number of days with snowfall and the 80th% ΔSWE, we use these parameters to characterize accumulation seasons of synthetic data. We identify sites with similar distributions of ΔSWE by using a chi-square test because the data is intrinsically binned by the 0.1 in. precision in ΔSWE. In this comparison, we ignore the number of days in the accumulation season with ΔSWE = 0 because they do not contribute either positively or negatively to the maximum SWE. Sites with similar ΔSWE distributions also provide values of 80th% ΔSWE.

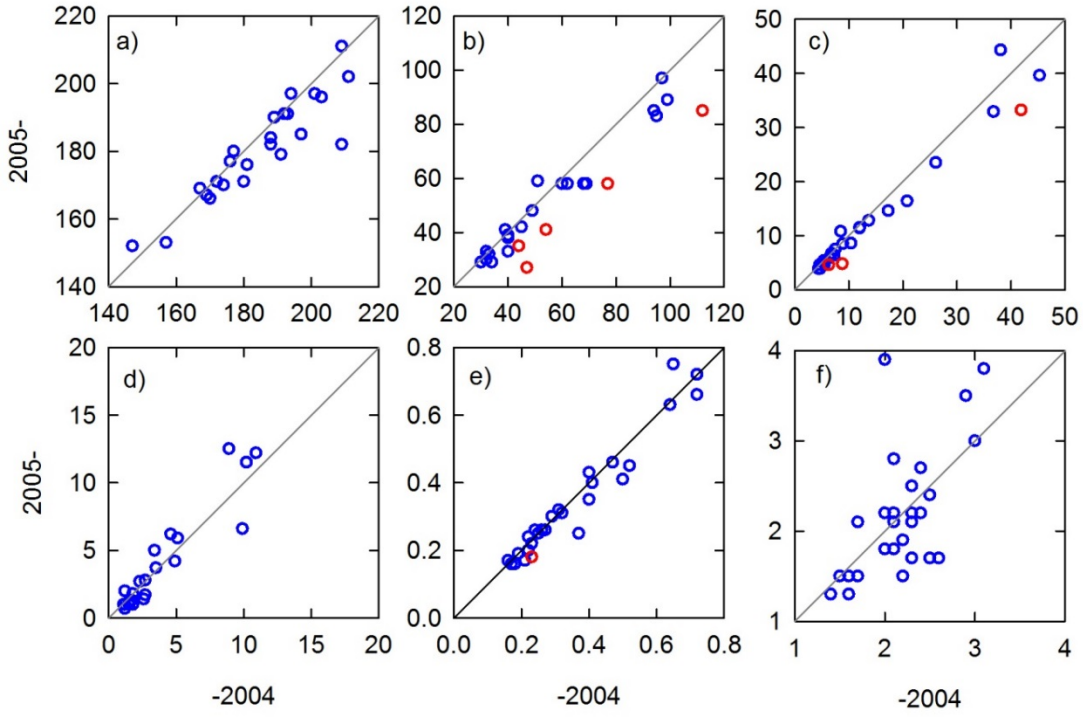

Figure 19. Comparison of accumulation season SWE for the period through 2004 (-2004) and the period from 2005 on (2005-) for the SNOTEL sites (*a*) mean number of days in accumulation season, (*b*) mean number of snowfall days in the accumulation season, (*c*) mean annual maximum SWE (in.), (*d*) mean absolute deviation from the mean annual maximum SWE (in.), (*e*) mean annual 80th% ΔSWE (in.) on days with snowfall, and (*f*) mean e^2-folding lag (day) for daily ΔSWE. Sites with significantly different means (5% level) are shown in *red*.

To compare the site distributions of the number of snow days in the accumulation season, we use the Kolmogorov-Smirnov test. Distributions of samples are generally assumed to be different if the probability that they were drawn from the same population is less than either 5% or 1%. For the distribution of snow days, we assume that samples are drawn from the same population if

that probability is 40% or greater. For the distribution of ΔSWE, our initial criterion for choosing similar sites is that the probability be 40% or higher. That sometimes results in no sites chosen. In those cases, we relax that criterion and use the site with the highest probability greater than 5%. Some sites are still left with no similar sites. Figure 20 shows the site relationships for both criteria. Note that there is little overlap in similar sites; that is, for a given site, the sites that are similar based on the distribution of the number of days with snowfall tend to be different from the sites that are similar based on the distribution of the daily ΔSWE. For the number of days with snowfall, more than three-quarters of the sites have at least three similar sites, half have at least five similar sites, and one-quarter have at least seven similar sites (maximum 11). One site (Turnagain Pass) has none. For the daily ΔSWE distribution, more than three-quarters of the sites have at least one similar site, but fewer than half have two or more similar sites, and fewer than one-quarter have at least three similar sites (nine maximum). Ten of the sites have only one similar site, and for nine of them that site was chosen by resorting to the 5% minimum criterion. Five sites, including Turnagain Pass, have no similar sites. These lone sites tend to be at either relatively low or relatively high elevations compared to other sites in their county or are the only site in the county (Long Lake in Juneau County). The distribution of days with snowfall for McNeil Canyon alone and with the five similar sites is shown in Figure 21. A histogram of the daily positive and negative ΔSWE for McNeil Canyon alone and combined with the two similar sites is shown in Figure 22a. The similar sites also provide an expanded set of values for the 80th% ΔSWE, with a cumulative distribution shown in Figure 22b.

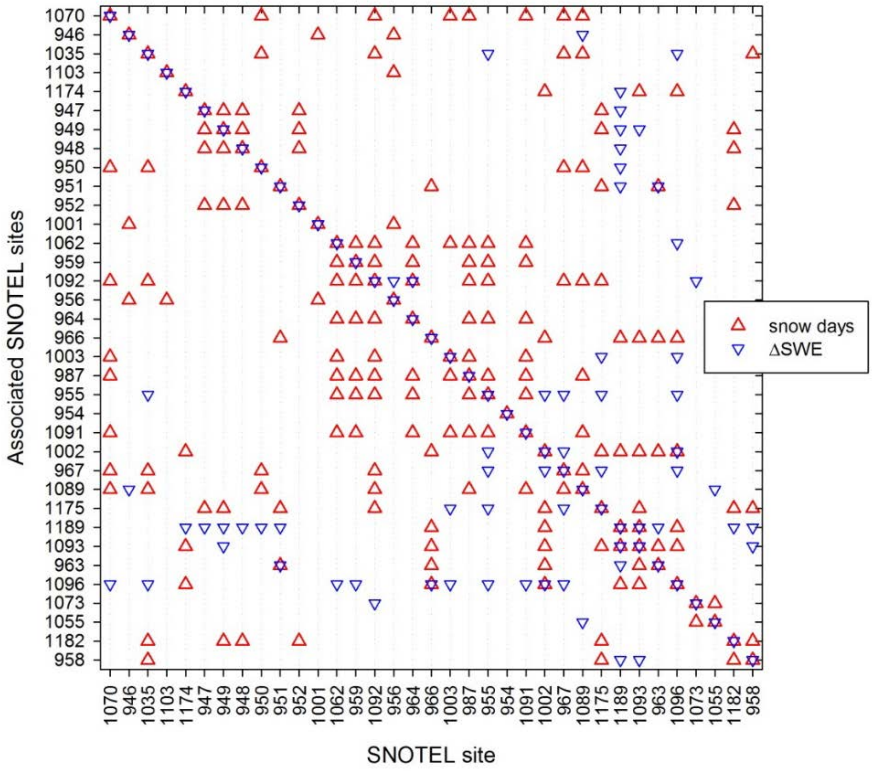

Figure 20. Relationships among SNOTEL sites. Sites are listed by their number in the same order as in Table 1. Sites with similar distributions of days with snowfall are indicated by Δ, and sites with similar ΔSWE distributions are shown with an upside-down Δ.

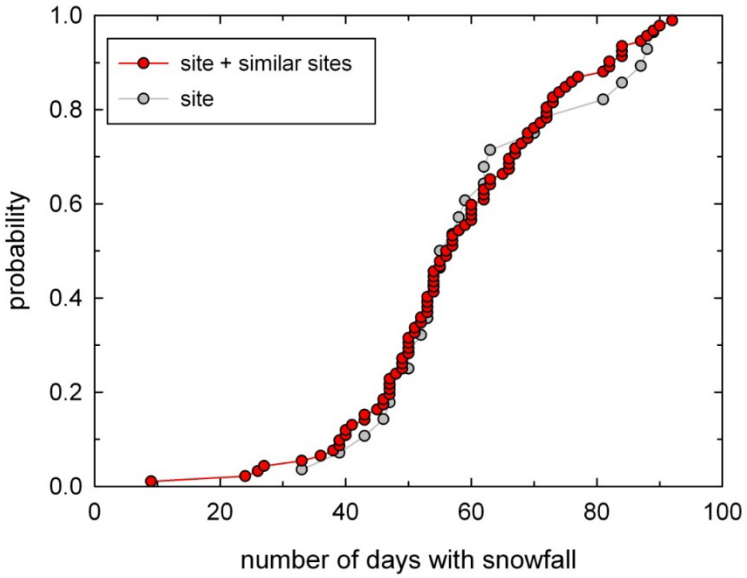

Figure 21. Cumulative distribution of the number of days with snowfall for McNeil Canyon and McNeil Canyon combined with five similar sites.

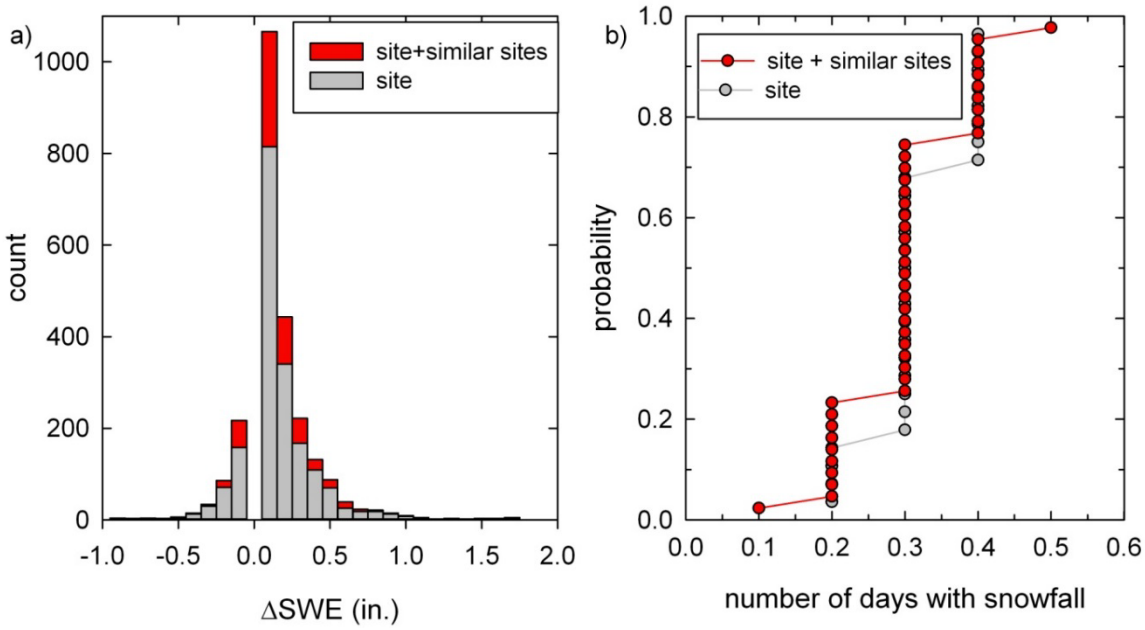

Figure 22. McNeil Canyon (*a*) histograms of ΔSWE for the site alone and combined with the two similar sites and (*b*) associated cumulative distribution of 80th% ΔSWE.

North American Regional Reanalysis

Figure 23 shows the same correlations of the maximum SWE with accumulation season characteristics for the NARR data as is shown for the SNOTEL sites in Figure 17. Compared to the SNOTEL sites, the NARR correlations of maximum SWE with 80th% ΔSWE tend to be

lower and are even negative, but not significant, at a number of points (Figure 23a). These lower correlations may be a result of the relatively noisy NARR data.

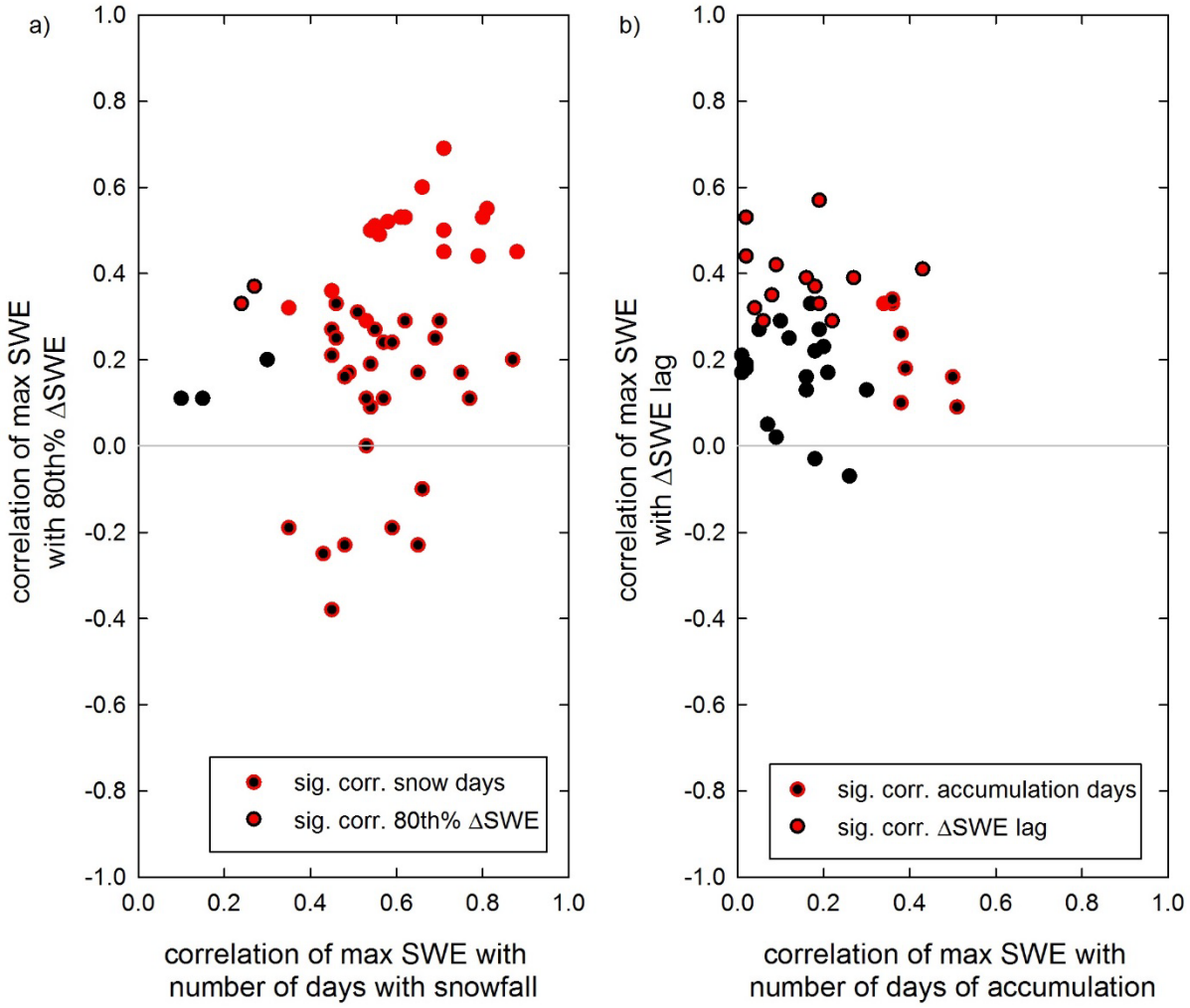

Figure 23. Correlations of the annual maximum SWE with various characteristics of the accumulation season for the 53 NARR grid points. Significant correlations are shown by a *red outline*, *red fill*, or *both*.

Mean values of SWE characteristics for the NARR data in the pre-AA era (25 years) and AA era (10 years) are compared in Figure 24, which is in the same format as Figure 19 for SNOTEL data. Means that are significantly different (5% level) are indicated by red symbols. The sites with significantly different values tend to have more snowfall days and higher maximum SWE in the AA era than in the pre-AA era. Similarly, the significant absolute max SWE deviations tend to be higher in the AA era than earlier, while 80th% ΔSWE are smaller. However, as we saw for the SNOTEL sites, there are few points with significant differences. This may be because AA does not have a significant effect on snow accumulation or because of our relatively short periods of record, particularly the 10 years representing the AA era.

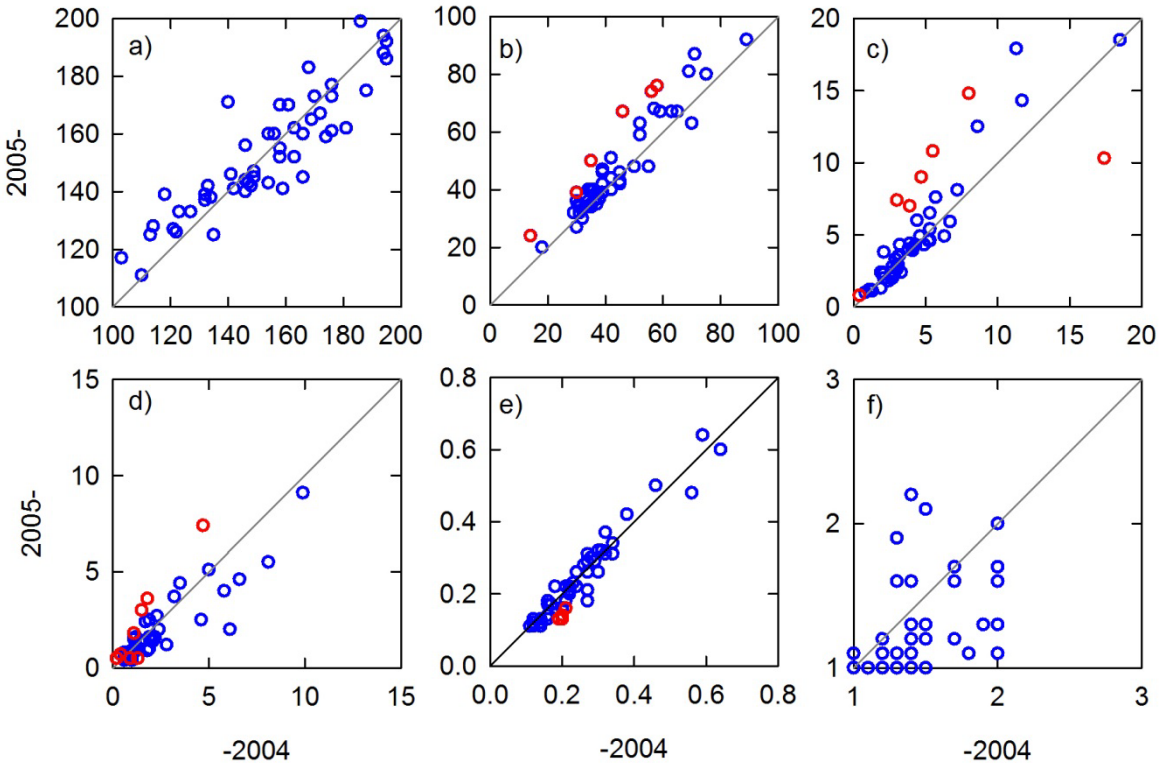

Figure 24. Comparison of accumulation season SWE for the period -2004 and the period 2005- for the 54 NARR grid points: (*a*) number of days in the accumulation season, (*b*) number of snowfall days in the accumulation season, (*c*) annual maximum SWE (in.), (*d*) absolute deviation from the mean annual maximum SWE (in.), (*e*) annual 80th% ΔSWE (in.) on days with snowfall, and (*f*) e^2-folding lag (day) in autocorrelation of daily ΔSWE. Sites with significantly different means (5% level) are shown in *red*.

For the number of days with snowfall, three-quarters of the 54 unique NARR points are similar to at least four other NARR points, half have at least nine similar points, and one-quarter have at least 13 similar points (18 maximum). One point, representing the Valdez NWS station, is similar to none of the other NARR points. For the daily ΔSWE distribution, two-thirds of the NARR points have at least one similar point, but only 20% have two or more (seven maximum) similar points. For 17 NARR points, there are no other points with similar ΔSWE distributions; and 17 of the 26 points with a single similar site were chosen by invoking the 5% minimum criterion.

Pan-Arctic Snow Reanalysis

Figure 25 shows the same correlations of the maximum SWE with accumulation season characteristics for the PASR data as is shown for the SNOTEL data in Figure 17 and the NARR data in Figure 23. The correlation of the max SWE with the number of days with snowfall is significant at all the PASR points.

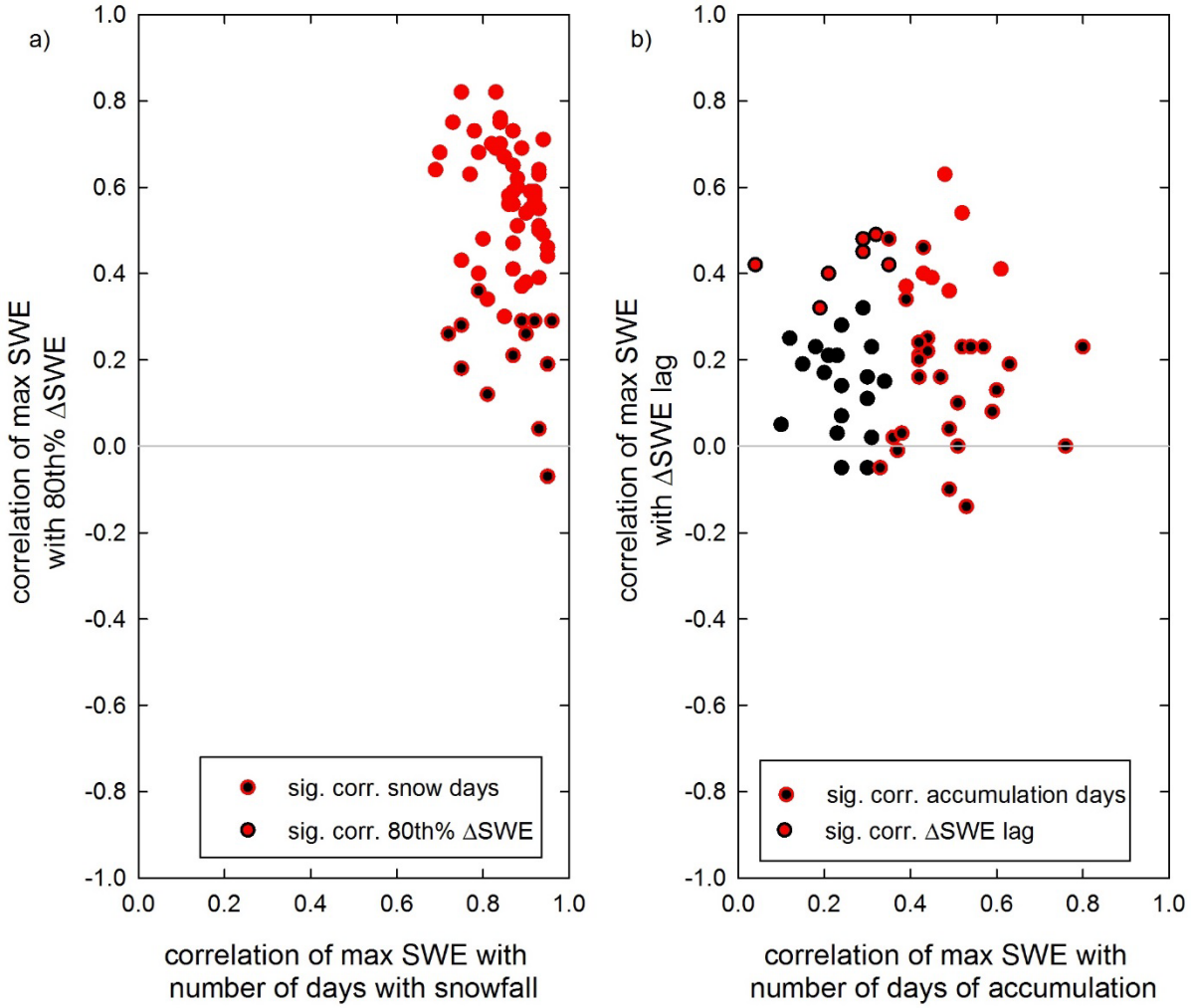

Figure 25. Correlations of the annual maximum SWE with various characteristics of the accumulation season for the 63 PASR grid points. Significant correlations are shown by a *red outline*, *red fill*, or *both*.

Mean values of SWE characteristics for the PASR data in the pre-AA era (25 years) and AA era (5 years) are compared in Figure 26, which is in the same format as Figure 19 for SNOTEL data and Figure 24 for the NARR data, with means that are significantly different indicated by red symbols. The significant differences in means tend to be more days with snowfall, higher annual max SWE, higher 80th% ΔSWE, and longer lags in the AA-era than before 2005. As we saw for the SNOTEL sites and NARR points, there are few points with significant differences between the two eras. Again, this may be because AA does not have a significant effect on snow accumulation or because of our relatively short periods of record, particularly the AA era, which is represented by only 5 years of data. The highest average annual max SWE for the PASR point representing Long Lake near Juneau are just under 100 in.

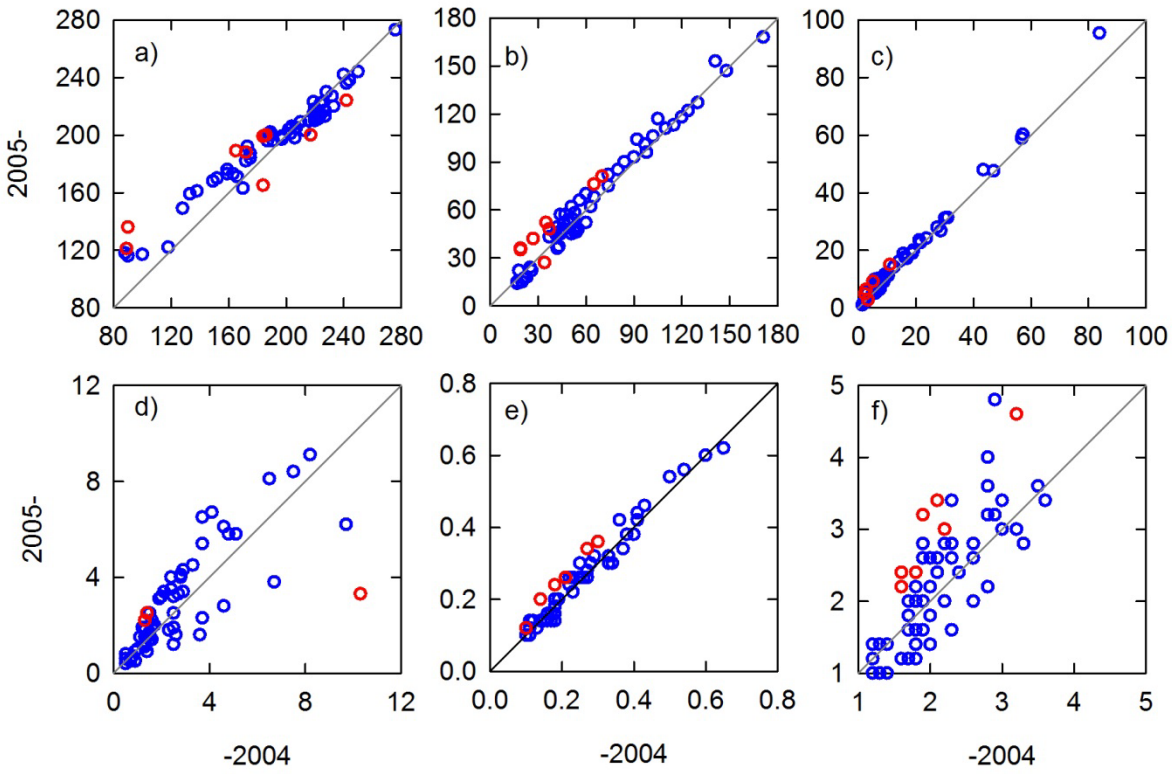

Figure 26. Comparison of accumulation season SWE for the period -2004 and the period 2005- for the 63 PASR grid points: (*a*) number of days in the accumulation season, (*b*) number of snowfall days in the accumulation season, (*c*) annual maximum SWE (in.), (*d*) absolute deviation from the mean annual maximum SWE (in.), (*e*) annual 80th% ΔSWE (in.) on days with snow, and (*f*) e^2-folding lag (day) in autocorrelation of daily ΔSWE. Sites with significantly different means (5% level) are shown in *red*.

For the number of days with snowfall, three-quarters of the 63 PASR points have distributions similar to at least two other PASR points, half have at least three similar points, and one-quarter have at least seven similar points (14 maximum). Two points, representing the Barter Island NWS station and the Upper Tsaina River SNOTEL site, have distributions of days with snowfall that are similar to none of the other PASR points. For the daily ΔSWE distribution, 70% of the PASR points have at least one similar point, but only 30% have two or more (five maximum) similar points. For 19 PASR points, there are no other points with similar ΔSWE distributions. Twelve of the 25 points for which a single similar site was chosen were picked by invoking the 5% minimum criterion. Compared to the SNOTEL and NARR data, the PASR points have more dissimilar accumulation season characteristics.

Synthetic Data

Synthetic SNOTEL and NARR data for the same locations near Fairbanks and Homer and in the same format as in Figure 11 are shown in Figure 27. There are two differences between Figure 27 and Figure 11: (a) Figure 27 represents only the accumulation season rather than the whole year, and (b) the synthetic winters in Figure 27 are random with no association between the

locations. Thirty-six years of synthetic data based on the PASR data are shown in Figure 28 for the same sites and format as in Figure 13

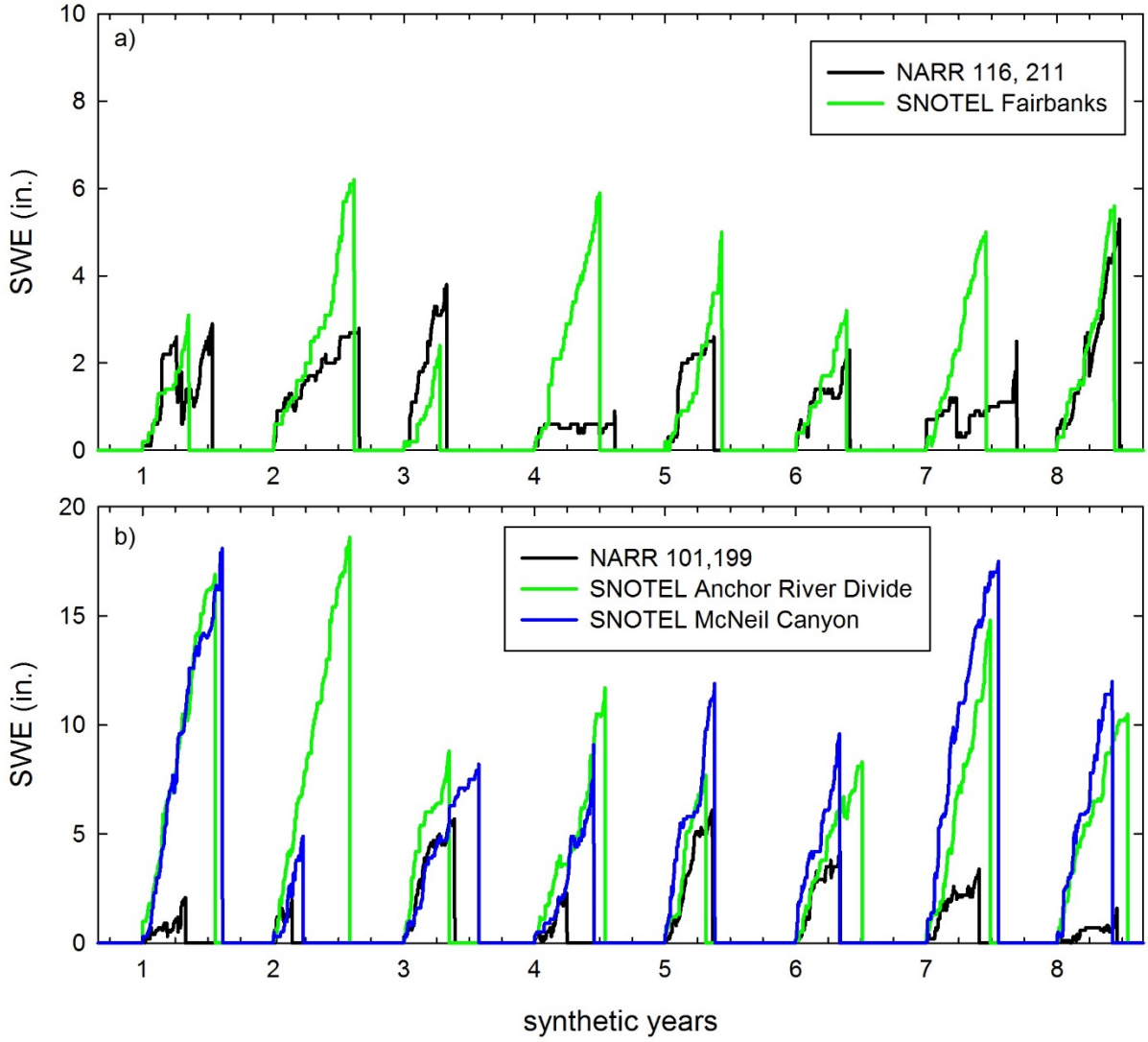

Figure 27. Eight years of synthetic time series for the SWE accumulation season for NARR grid points and corresponding SNOTEL sites near (*a*) Fairbanks and (*b*) Homer. The synthetic data exhibit the relatively noisy daily changes in the NARR data compared to SNOTEL data.

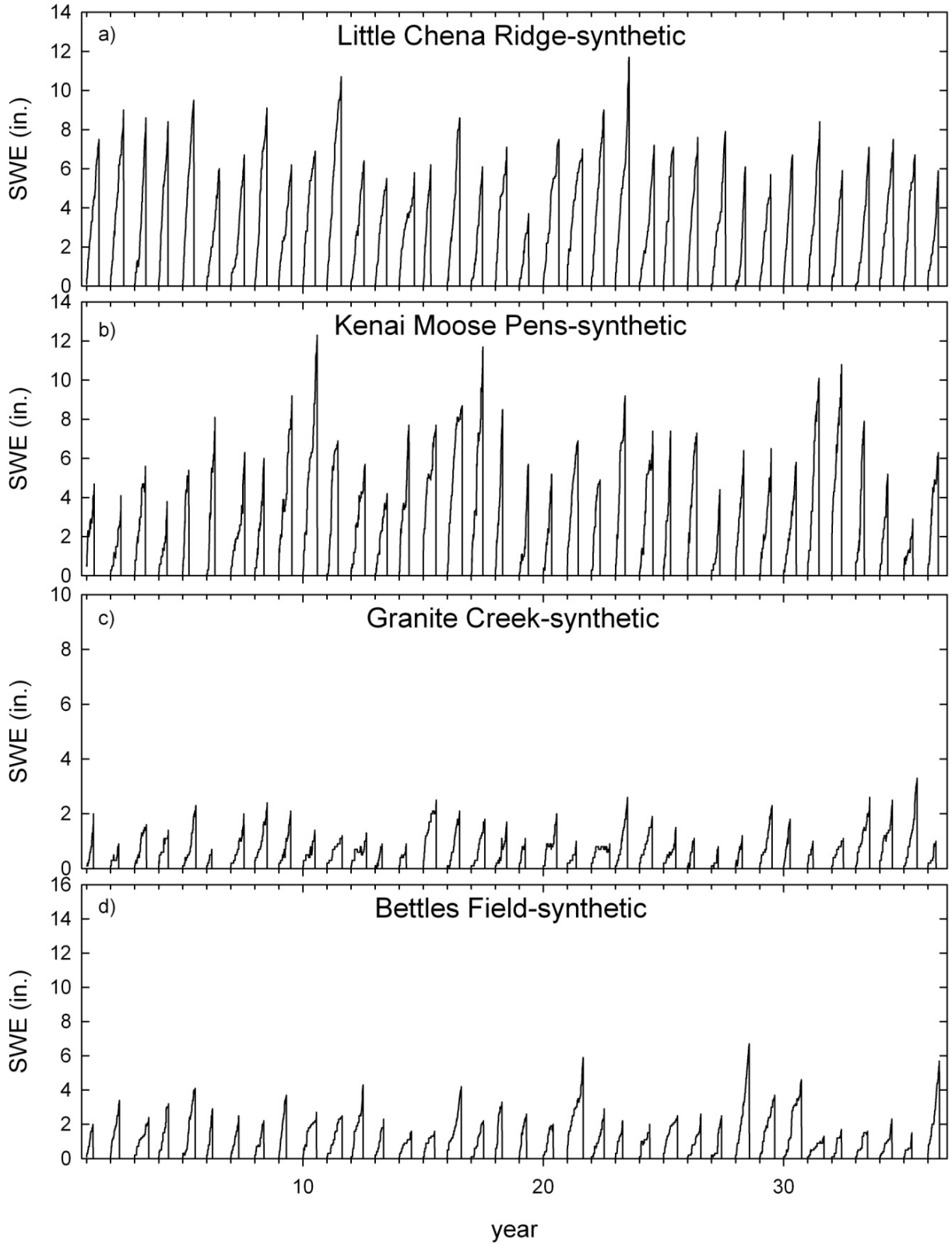

Figure 28. Synthetic SWE data for the accumulation season based on the characteristics of PASR data for the same locations as in Fig. 13.

Figure 29 plots the correlation of max SWE with 80th% ΔSWE vs. the correlation of max SWE with the number of days with snowfall in the accumulation season for synthetic data for both the pre-AA and AA eras in for synthetic SNOTEL data, NARR data, and PASR data. Like measured data, the synthetic data show a greater correlation of max SWE with the number of days with snowfall than with the 80th% ΔSWE. For the 499 years of synthetic data, all these correlations are significant. The correlation of the number of days with snowfall with 80th% ΔSWE is shown in Figure 29d. We chose those two parameters independently for each accumulation season so the correlations are small, as expected.

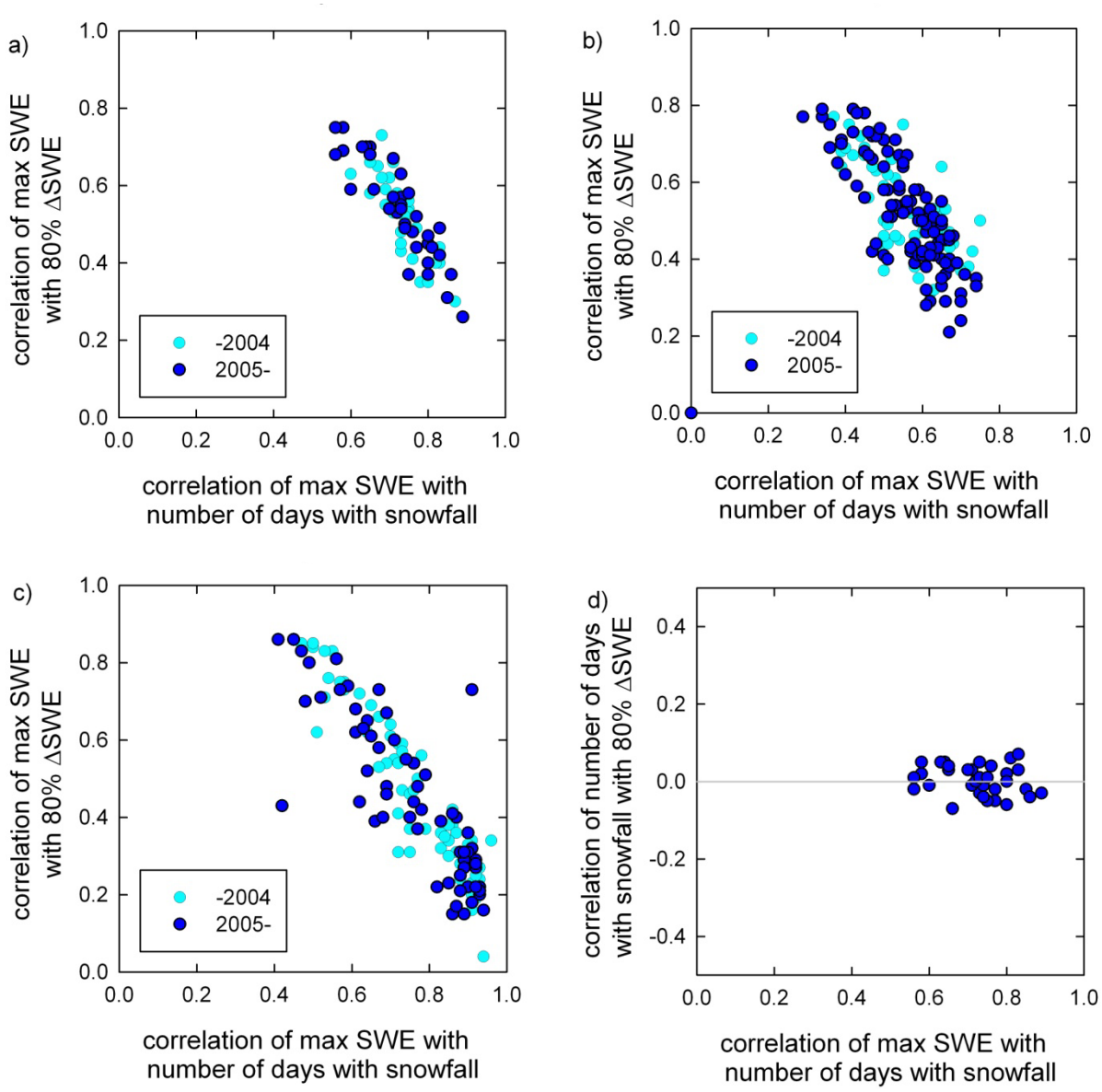

Figure 29. Max SWE correlations for synthetic data for the pre-AA and AA eras for (*a*) SNOTEL, (*b*) NARR, and (*c*) PASR. The lack of correlation between the number of days with snowfall and 80th% ΔSWE is shown in (*d*) for the synthetic SNOTEL data.

Extreme Value Analysis

For the synthetic SNOTEL data, the GEV, LN3, and PE3 distributions were acceptable for two-thirds of the sites for both eras. However, for the pre-AA era, the GLO distribution was the only one acceptable for two sites; and none of the 3-parameter distributions was acceptable at three sites. In the AA era, ten of the sites had no acceptable 3-parameter distributions. Figure 30 shows some of the synthetic data and fitted 3-parameter and kappa distributions. The mean recurrence interval on the horizontal axis is defined as the inverse of the probability of exceedance of the normalized SWE in any year. So, for example, a load with a 1% probability of being exceeded in any year has a mean recurrence interval of 100 years. The axis scale in Figure 30 is chosen so that a Gumbel distribution would plot as a straight line. Lines that curve up, like the GLO distribution in Figure 30c, have a longer tail than the Gumbel distribution; and lines that curve down, like the GPA distribution, have a shorter tail. The examples in Figure 30 were chosen to illustrate the variety of results we obtained, with only GLO acceptable in (a); GEV, PE3, and LN3 acceptable in (b); and none acceptable in (c). In all cases, the 4-parameter kappa distribution provides a good fit to the data.

For the 53 NARR grid points, the GEV, LN3, and PE3 distributions provided acceptable fits for three-quarters of the pre-AA era points and two-thirds of the AA-era points. At one point pre-AA and two other points in the AA era, the GPA distribution was the only one acceptable. At nine points in both eras, none of the 3-parameter distributions was acceptable. Only two of those locations were the same in the two eras. The plots in Figure 31 show the synthetic data and fitted distributions for both eras for the NARR grid representing the Anchorage NWS station and Elmendorf AFB. Pre-AA, only the GPA distribution was acceptable; and in the AA era, none of the 3-parameter distributions was acceptable.

The GEV, LN3, and PE3 distributions provided acceptable fits for two-thirds of 63 PASR grid points in the pre-AA era and for almost half of the grid points the AA era. The GPA distribution was the only acceptable one for four points pre-AA and three points in the AA era, while the GLO distribution was the only acceptable one for one point in each era. None of the 3-parameter distributions was acceptable for 15% of the points pre-AA and 40% in the AA era. The two PASR grid points representing the Yakutat NWS station are plotted for the AA era in Figure 32. None of the 3-parameter distributions was acceptable for these points. Note the significant difference in results for these adjacent PASR points.

Because of the variety of acceptable 3-parameter distributions in our results and the lack of acceptable 3-parameter distributions for many locations, we used the 4-parameter kappa distribution to estimate extremes and compare the pre-AA and AA eras. Confidence intervals for synthetic data at two SNOTEL sites representing the widest and narrowest intervals are shown in Figure 33. Distributions with long tails, as in Figure 33a, have wider confidence intervals than those with short tails, as in Figure 33b. Typical confidence intervals for a 50-yr mean recurrence interval for all the synthetic data are ±5%.

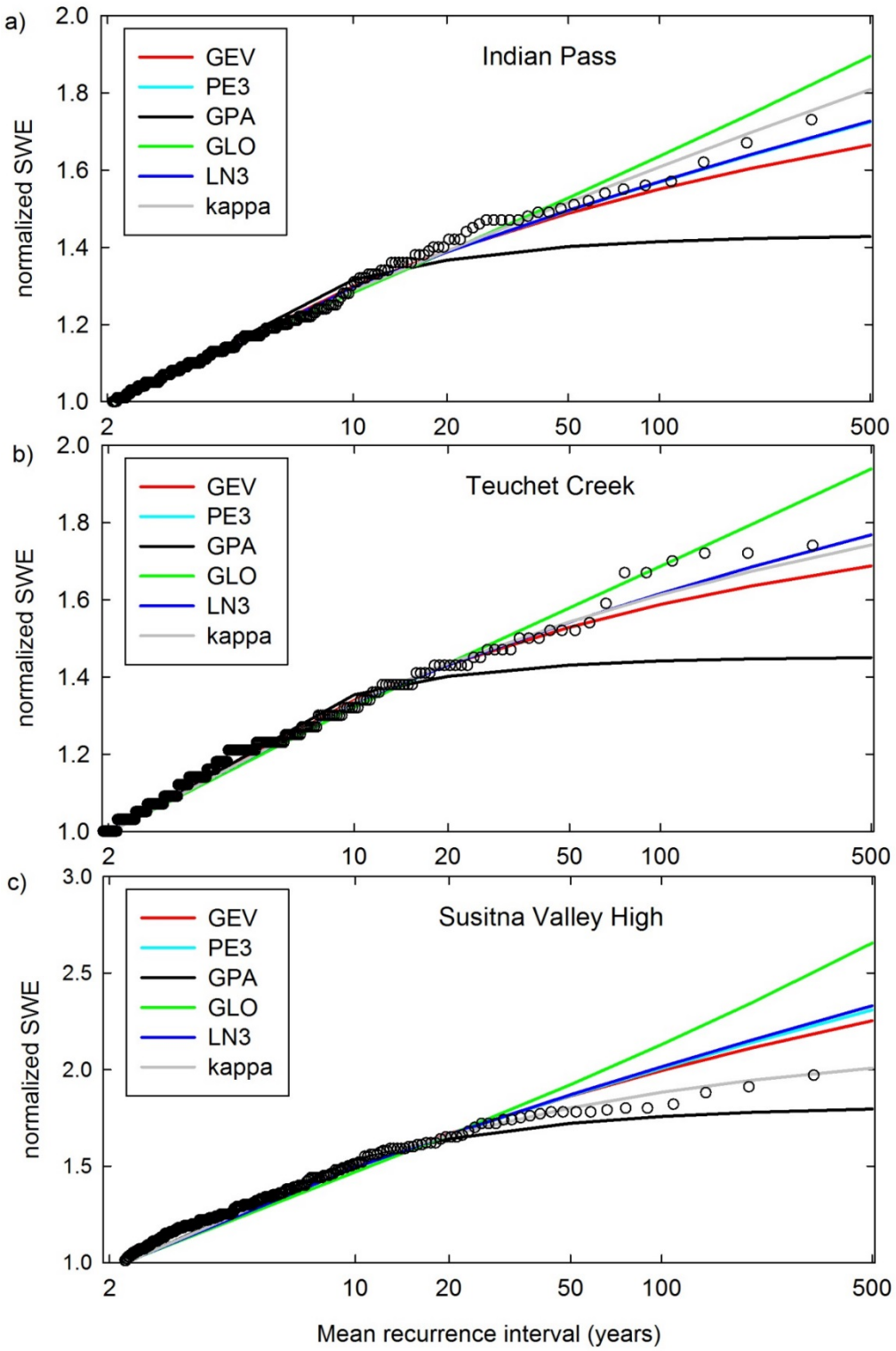

Figure 30. Kappa distribution and the five 3-parameter distributions fitted to synthetic SNOTEL data at three sites for the pre-AA era: (*a*) GLO is acceptable; (*b*) GEV, PE3, and LN3 are acceptable; (*c*) none of the 3-parameter distributions is acceptable.

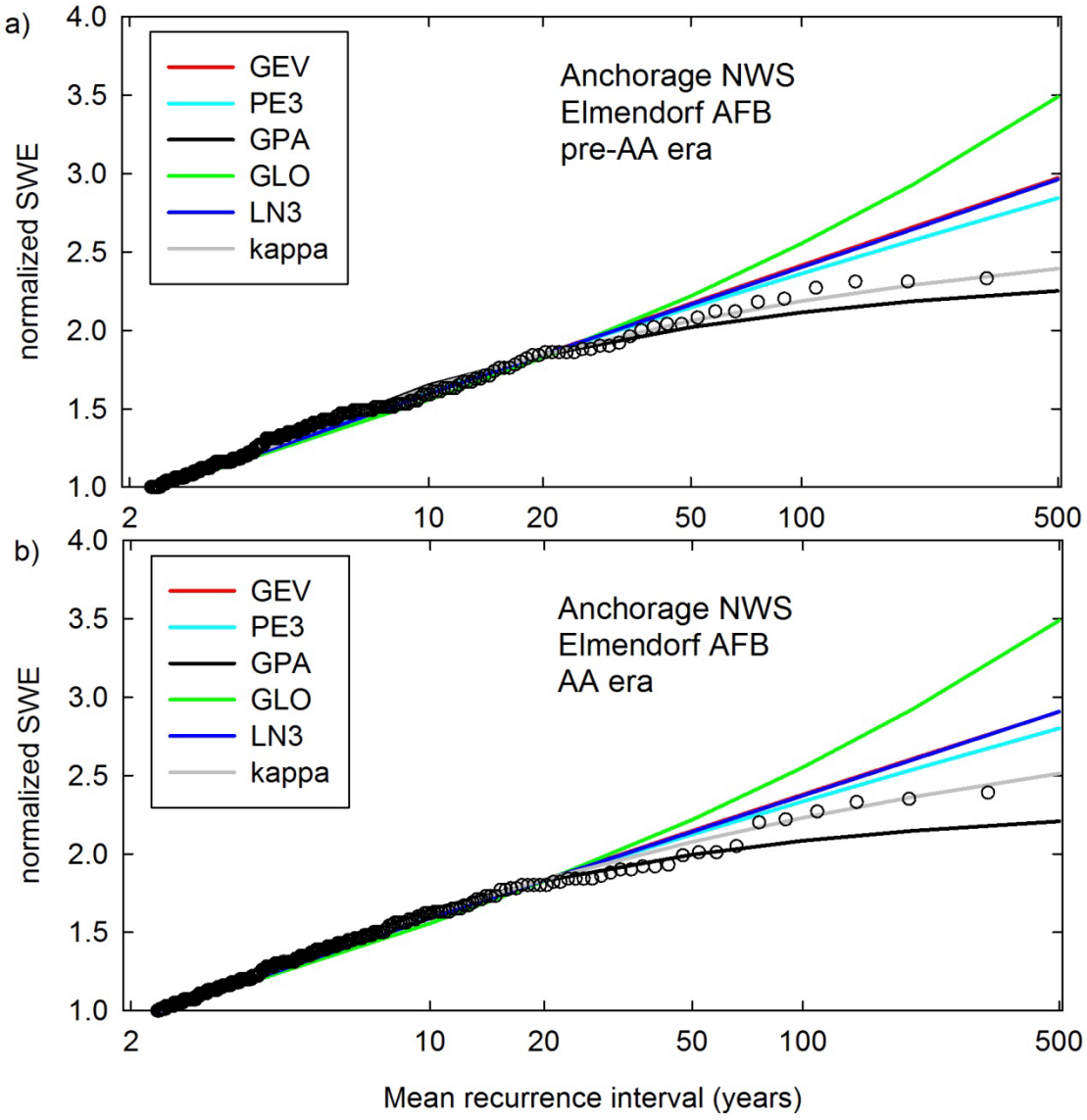

Figure 31. Kappa distribution and the five 3-parameter distributions fitted to synthetic NARR data representing the Anchorage NWS station and Elmendorf AFB: (*a*) pre-AA era, GPA is acceptable, and (*b*) AA era, none of the 3-parameter distributions is acceptable.

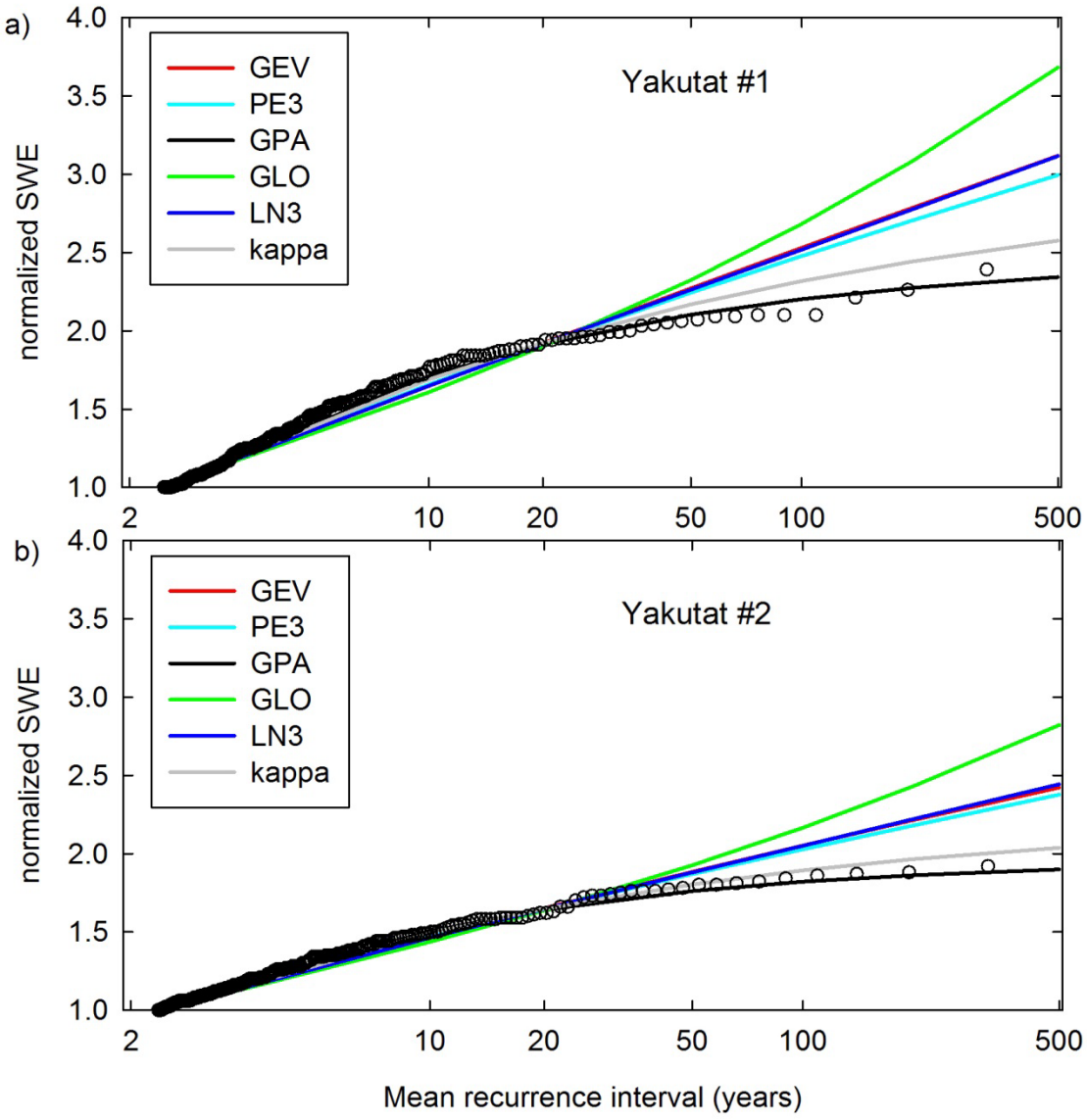

Figure 32. Kappa distribution and the five 3-parameter distributions fitted to synthetic PASR data at two grid points representing the Yakutat NWS station in the AA era. None of the 3-parameter distributions is acceptable in either case.

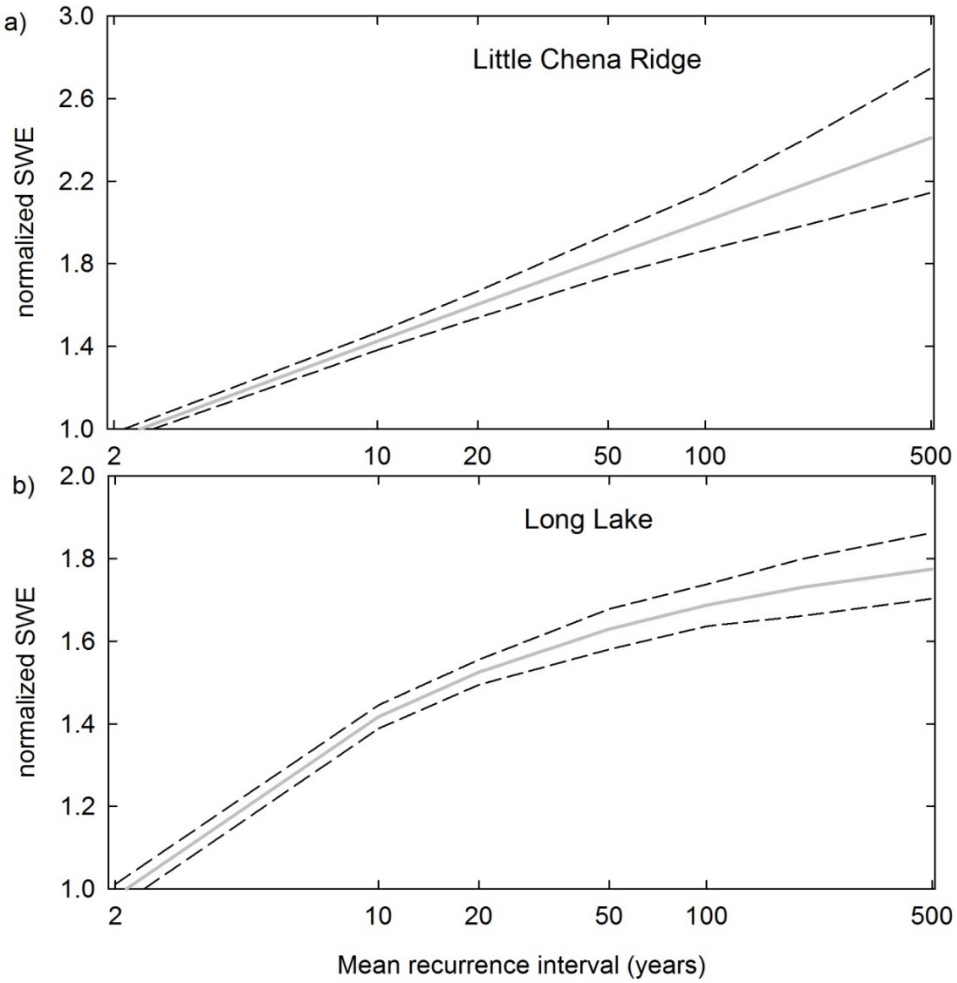

Figure 33. Comparison of confidence intervals for kappa distribution fits to synthetic SNOTEL data. The confidence intervals are wider for distributions with (*a*) long tails than (*b*) short tails.

SWE for a 50-year mean recurrence interval comparing the AA era with the pre-AA era are shown in Figure 34 for all three sets of synthetic data. Most AA-era values are within 10% of the pre-AA value for that location and are therefore within the confidence intervals. For the SNOTEL data, AA-era values that are different from the pre-AA values by more than 10% tend to be smaller (15 smaller, 2 larger). However, for the NARR and PASR locations, the opposite is true. For the NARR data, the distribution of values differing by more than 10% is 4 smaller and 13 larger; and for the PASR data, it is 2 smaller and 15 larger. The spatial distribution of the change in the 50-year SWE is shown in Figure 35 for the three synthetic datasets. For each location, we also determined the mode of the tendency for significantly smaller, no change, or significantly larger 50-year SWE for each location for the three synthetic datasets. If two or more of the datasets exhibited the same tendency, that result is plotted in Figure 35d. For the locations with a majority tendency, the 50-year SWE either remains the same in the AA era as in the pre-AA era or increases with no apparent spatial delineation of those tendencies. With the exception of the Upper Tsaina River location (at 1209 m near Valdez), the other locations with a tendency toward higher SWE in the AA era are at relatively low elevations.

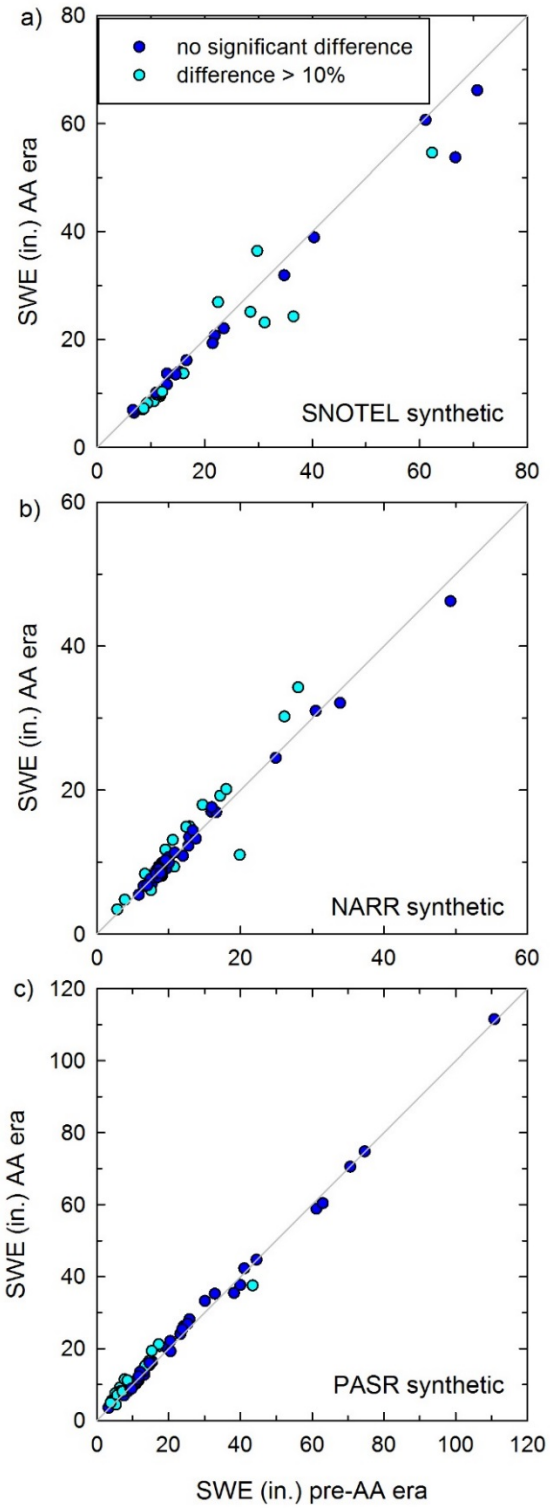

Figure 34. SWE for a 50-year mean recurrence interval for the AA era compared to the pre-AA era calculated from synthetic data (*a*) SNOTEL, (*b*) NARR, and (*c*) PASR. At most sites, the difference in values is less than the width of the confidence intervals.

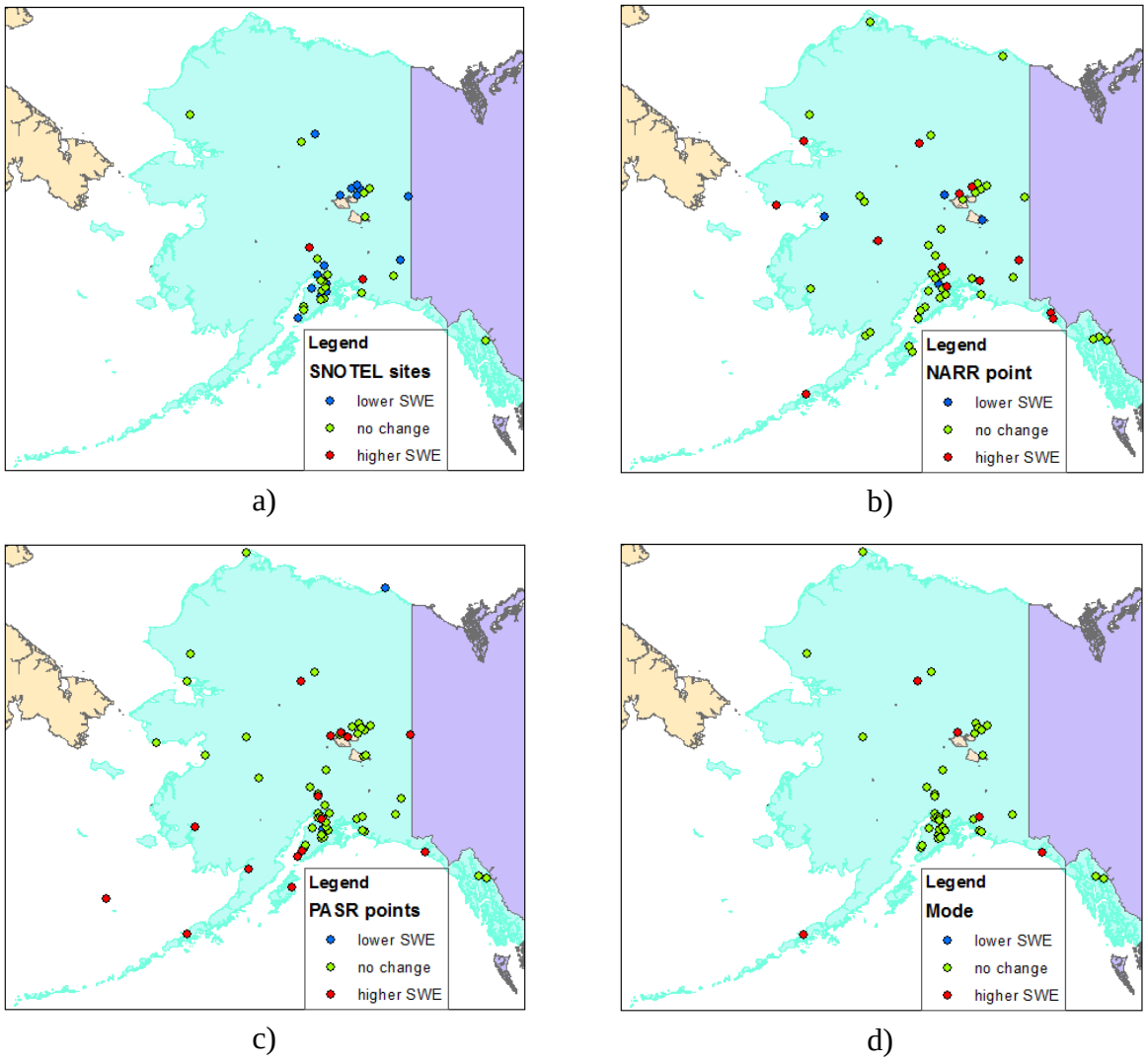

Figure 35. Change in the SWE for a 50-year MRI in the AA era compared to the pre-AA era, based on (*a*) synthetic SNOTEL data; (*b*) synthetic NAA data; (*c*) synthetic PASR data; and (*d*) mode of the SNOTEL, NARR, and PASR results.

Global Climate Model

The AA resulting in a decreased equator-to-pole temperature gradient is hypothesized to cause more persistent weather patterns in the midlatitudes. The primary purpose of this project was to determine if this greater persistence is manifested in the winter snow accumulation season in Alaska as a greater variation from year to year in snow loads and a corresponding increase in extreme ground snow loads. A secondary effort in the project was the analysis of annual maximum SWE from a GCM to evaluate the change in 50-year snow loads over the twenty-first century that were associated with global climate change.

The trend in the 50-year MRI SWE as the percent change per decade is plotted for Alaska in Figure 36 for the Hadley model and in Figure 37 for the INM model for RCPs 4.5 and 8.5. In both figures, the results are based on the GEV distribution, but the LN3 distribution provides

essentially the same results. For example, for INM-CM4 RCP 8.5, the typical absolute difference in the 50-year MRI SWE for the GEV and LN3 distributions is less than 0.5 in.; and the typical absolute difference in the trend is less than 0.5% per decade. The two GCMs behave significantly differently. The Hadley model in Figure 36 for RCP 4.5 shows a high rate of decreasing 50-year SWE in the southern coastal region of Alaska and a high rate of increasing SWE in interior and northern Alaska. For RCP 8.5, the rates of both trends are increased. In contrast, the INM model for RCP 4.5 (Figure 37) shows a moderate trend of decreasing 50-year SWE in the southern half of Alaska and a slight increasing trend in the northern half of the state. For RCP 8.5, the decreasing trend covers almost the entire state; and the rate is increased compared to RCP 4.5 but is substantially smaller than shown by HadGEM2-AO.

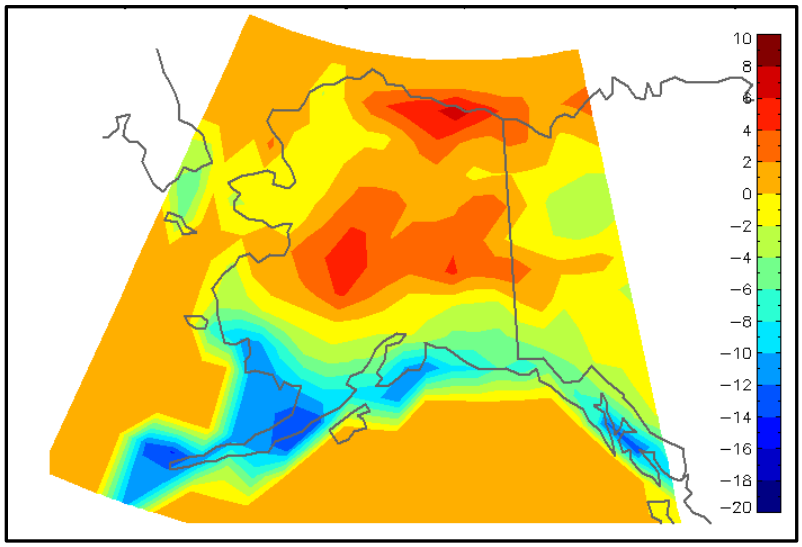

a)

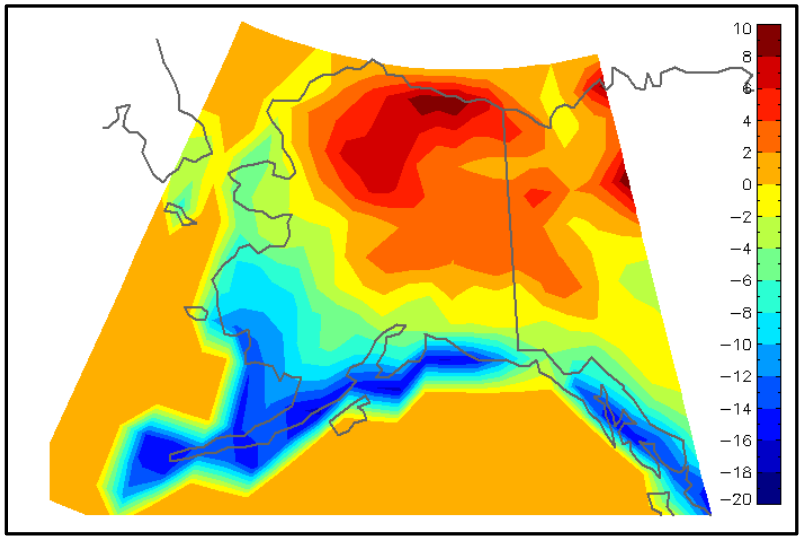

b)

Figure 36. Percent change in SWE per decade in the twenty-first century for a 50-year MRI based on CMIP5 model HadGEM2-AO for (*a*) RCP 4.5 and (*b*) RCP 8.5.

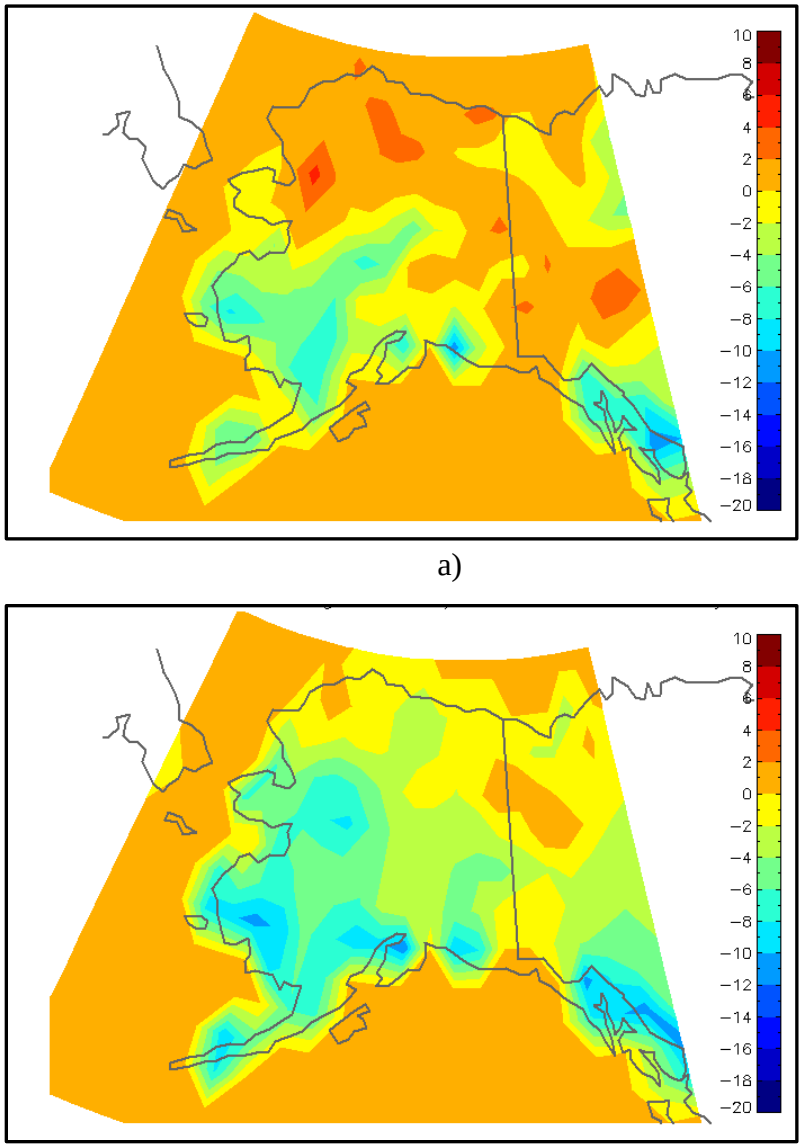

a)

b)

Figure 37. Percent change in SWE per decade in the twenty-first century for a 50-year MRI based on CMIP5 model INM-CM4 (*a*) RCP 4.5 and (*b*) RCP 8.5.

Summary

For the primary effort in this project, we obtained SWE data from four sources, intending to use the characteristics of those datasets to generate long periods of record of synthetic data to use in an EVA for estimating SWE for a 50-year mean recurrence interval. We did not ultimately use the SWE data from the NWS, both because only one station in Alaska had SWE data for recent years and also because SWE appears to be frequently estimated from the measured snow depth rather than measured. Thus, the calculated daily SWE increments might be a result of an estimated SWE followed by a measured SWE rather than representing snowfall or snow melt. The three remaining datasets represent (a) SWE measurements made automatically at SNOTEL

sites and quality controlled by the NRCS; (b) SWE on a 32 km grid, originating with the Air Force Weather Agency daily snow depth analysis; and (c) SWE on a 10 km grid obtained by downscaling weather parameters from the MERRA reanalysis product and modeling snowfall, accumulation, and melting.

Statistical analyses of the data showed that the annual maximum SWE tends to correlate with the number of days in the accumulation season with snowfall (daily $\Delta SWE > 0$) and the 80th% daily positive ΔSWE and that these two parameters are not correlated. We created synthetic accumulation seasons for each of our SNOTEL, NWS, and military locations by using these characteristics of the accumulation seasons before AA, based on SWE data through 2004, and the seasons with AA, based on SWE data from 2005 to the end of the POR. We used the annual maximum SWE from the 499 synthetic years of data at each location in the EVA. A number of different 3-parameter extreme value distributions were acceptable for most locations and sources for the synthetic data; but for some, none of those distributions was acceptable. Therefore, we relied on the 4-parameter kappa distribution for the EVA at all locations.

We found that for all three sources of data, the 50-year SWE based on the synthetic data did not change significantly at the majority of locations from the pre-AA era to the AA era. However, 43% of the SNOTEL sites had smaller 50-year SWE during AA than before AA while 6% of the sites had larger values. At 24% of the NARR points, the 50-year SWE during AA was larger than before AA while the value was smaller at 7% of the points.

Similarly, at 24% of the PASR points, the 50-year SWE during AA was larger than before AA while 3% of the points had smaller 50-year SWE. There is no apparent spatial grouping of the locations with significant differences in the 50-year SWE before and during AA for any of the datasets.

The global climate models also do not provide consistent guidance on the trend in 50-year SWE. The results depend on the both the GCM and the specified RCP. For the British model, the significantly increasing trend in the northern half of Alaska and decreasing trend in the south are both amplified in an RCP 8.5 climate compared to an RCP 4.5 climate. For the Russian GCM, a slightly increasing trend in SWE in the north for RCP 4.5 changes to a neutral or slightly decreasing trend for RCP 8.5 while the slight negative trend in the south becomes more negative.

Conclusions and Implications for Future Research and Implementation

The analysis indicates little change in 50-year snow loads associated with AA, at least as AA is incorporated in the SWE measurements in the SNOTEL, NARR, and PASR datasets available to date. At the locations where the difference in SWE between the AA era and pre-AA era is greater than the width of the confidence interval, 50-year snow loads tend be smaller in the AA era than earlier for the SNOTEL-based synthetic data and larger for the NARR- and PASR-based synthetic data. The two GCM simulations we acquired are also inconclusive. Both models show an increasing trend in SWE in northern Alaska and a decreasing trend in southern Alaska for RCP4.5. That trend becomes significantly more pronounced for the British model with the

greater total radiative forcing in RCP 8.5 while for the Russian model the trend increases only slightly in the south and decreases or reverses in the north.

We might have obtained different results if we had defined the pre-AA era and AA era differently. In their paper investigating the signal of persistence associated with AA, Francis and Skific (2015) use 1979 to 1994 for the pre-AA era and 2000 to 2013 for the AA era in one analysis. In another they use 1948 to 1990 and 1996 to 2012, respectively. The examples of persistent winter weather that they cite are in recent years only, however, between 2009 and 2013. For this study, we initially chose the year 2000 as the beginning of the AA era and found no significant differences between any of the characteristics of the pre-AA and AA eras for any of the SNOTEL sites for that choice. Our subsequent choice of 2005 resulted in some significant differences. Dropping five years, ending the pre-AA era in 2000 and starting the AA era in 2005 is another possibility but would have resulted in very short AA-era datasets and more difficulty in identifying significant differences and creating synthetic data with the appropriate characteristics. Redoing this analysis in 10 or 20 years to have a longer POR and better definition of the characteristics of AA would be appropriate.

Alaska is a huge state with a long coastline and great variation in terrain and climate over short distances. Furthermore, snow load measurement sites, or even sites where snow depth is measured sites are few and far between compared to the lower 48 states. Because of this, 50-year snow loads in Alaska are not mapped in ASCE (2010) Standard 7 and will not be mapped in the 2016 revision of the Standard. Engineers designing buildings for military facilities at locations not included in ASCE (2010) Standard 7 Table 7.1 or UFC Table E2 do not have 50-year ground snow loads to use in design. The snow loads in those tables are only for the locations specified and do not apply to nearby locations. The investigation of SWE datasets to use for this project shed light on some of the issues around measured SWE. At most NWS first-order stations on most days, SWE is estimated by dividing the snow depth by ten, rather than actually being measured. Thus, any apparent daily variation, or the lack of variation, in the reported SWE may not be real. Reanalysis products assimilate those measurements and the measurements are also used in validating satellite observations and global climate model simulations of SWE. SWE is measured rather than estimated at SNOTEL sites. However these sites tend to be located in watersheds to track snow accumulation for water control during snow melt runoff and water supply planning and thus tend not to be located near cities or military bases.

The need for a snow load map for the entire state may become more acute if Alaska facilities are expanded to deal with the expected ship traffic through the Northwest Passage and Northern Sea Route with the retreat of the Arctic ice cover. Ideally, such a map would be based on gridded SWE with a grid spacing small enough to capture the variation in snow load with elevation in the mountains and distance from the coast. A dataset that provides the maximum SWE at each grid point each year, based perhaps on a combination of ground measurements, passive microwave data from satellites, and models of snow accumulation using weather data, would be ideal. Such a dataset might not reduce the uncertainty in changes in SWE associated with AA or global climate change but would quantify the expected large spatial variation in Alaska in design snow loads.

Literature Cited

Adams, E. 2012. Anchorage, Alaska Breaks Seasonal Snowfall Record. *Alaska Dispatch News*, 7 April. http://www.adn.com/anchorage/article/anchorage-alaska-breaks-seasonal-snowfall-record/2012/04/07/.

ASCE (American Society of Civil Engineers). 2010. *Minimum Design Loads for Buildings and Other Structures*. ASCE/SEI 7. Reston, VA: American Society of Civil Engineers.

Bromwich, D. H., A. B. Wilson, L. S. Bai, G. W. K. Moore, B. Kuo, Z. Liu, H.-C. Lin, and M. Barlage. 2014. A Comparison of the Regional Arctic System Reanalysis and the Global ERA-Interim Reanalysis for the Arctic. *Quarterly Journal of the Royal Meteorological Society* 142:644–658. doi:10.1002/qj.2527.

DOD (Department of Defense). 2014. *United Facilities Criteria (UFC): Structural Engineering*. UFC 3-301-01. Washington, DC: Department of Defense. http://www.wbdg.org/ccb/DOD/UFC/ufc_3_301_01.pdf.

Earth Observing Laboratory. 2016. *SnowModel Pan-Arctic Data 1979–2009*. Boulder, CO: National Center for Atmospheric Research, Earth Observing Laboratory. http://data.eol.ucar.edu/codiac/dss/id=106.309.

Ellingwood, B., and R. Redfield. 1983. Ground Snow Loads for Structural Design. *ASCE Journal of Structural Engineering* 109 (4): 950–964.

Francis, J., N. Skific. 2015. Evidence Linking Rapid Arctic Warming to Mid-Latitude Weather Patterns. Philosophical Transactions of the Royal Society A 373: 20140170. http://dx.doi.org/10.1098/rsta.2014.0170.

Francis, J. A., and S. J. Vavrus. 2012. Evidence Linking Arctic Amplification to Extreme Weather in Mid-Latitudes. *Geophysical Research Letters* 39 (6): L06801. doi:10.1029/2012GL051000.

Gayno, G., J. Woollen, K. Mitchell, B. Kistler. 2007. Snow Analysis for CFSRR. Presented at the First CFSRR Advisory Board Meeting, 7–8 November. http://cfs.ncep.noaa.gov/cfsreanl/PRESENTATION/20071107/CFSSR_SAB_Gayno.ppt.

Hosking, J. R. M.. 2005. *Fortran Routines for Use with the Method of L-Moments*, Version 3.04. RC 20525(09033) 8/5/96, revised 7/25/05. Yorktown Heights, NY: IBM Research Division.

Hosking, J. R. M., and J. R. Wallis. 1997. *Regional Frequency Analysis*. New York: Cambridge University Press.

Knutti, R., D. Masson, and A. Gettelman. 2013. Climate Model Genealogy: Generation CMIP5 and How We Got There. *Geophysical Research Letters* 40 (6): 1194–1199. doi:10.1002/grl.50256.

Lawrence Livermore National Laboratory. 2016. *ESGF@DOE/LLNL*. Livermore, CA: Lawrence Livermore National Laboratory. http://pcmdi9.llnl.gov/.

Liston, G., and K. Elder. 2006a. A Distributed Snow-Evolution Modeling System (SnowModel). *Journal of Hydrometeorology* **7**:1259–1276.

———. 2006b. A Meteorological Distribution System for High-Resolution Terrestrial Modeling (MicroMet). *Journal of Hydrometeorology* **7**:217–234.

Liston, G., and C. A. Hiemstra. 2011. The Changing Cryosphere: Pan-Arctic Snow Trends (1979–2009). *Journal of Climate* 24:5691–5712. doi:10.1175/JCLI-D-11-00081.1.

Meinshausen, M., S. J. Smith, K. Calvin, J. S. Daniel, M. L. T. Kainuma, J. F. Lamarque, K. Matsumoto, S. A. Montzka, S. C. B. Raper, K. Riahi, A. Thomson, G. J. M. Velders, and D. P. P. van Vuuren. 2011. The RCP Greenhouse Gas Concentrations and Their Extensions from 1765 to 2300. *Climatic Change* 109:213–241. doi:10.1007/s10584-011-0156-z.

Menne, M. J., I. Durre, R. S. Vose, B. E. Gleason, and T. G. Houston. 2012a. An Overview of the Global Historical Climatology Network–Daily Database. *Journal of Atmospheric and Oceanic Technology* 29:897–910. doi:10.1175/JTECH-D-11-00103.1.

Menne, M. J., I. Durre, B. Korzeniewski, S. McNeal, K. Thomas, X. Yin, S. Anthony, R. Ray, R. S. Vose, B. E.Gleason, and T. G. Houston. 2012b. *Global Historical Climatology Network–Daily (GHCN-Daily), Version 3.20*. NOAA National Climatic Data Center doi:10.7289/V5D21VHZ. http://www.ngdc.noaa.gov/docucomp/page?xml=NOAA/NESDIS/NCDC/Geoportal/iso/xml/C00861.xml&view=getDataView&header=none (accessed October 2015).

Mesinger F., G. DiMego, E. Kalnay, P. Shafran, W. Ebisuzaki, D. Jovic, J. Woollen, K. Mitchell, E. Rogers, M. Ek, Y. Fan, R. Grumbine, W. Higgins, H. Li, Y. Lin, G. Manikin, D. Parrish, and W. Shi. 2006. North American Regional Reanalysis. *BAMS* 87 (3): 343–360. doi:10.1175/BAMS-87-3-343.

Met Office. 2016. *Met Office Climate Preditction Model: HadGEM2 Family*. Exeter, UK: Met Office. http://www.metoffice.gov.uk/research/modelling-systems/unified-model/climate-models/hadgem2.

NCEP (National Centers for Environmental Prediction), National Weather Service, National Oceanic and Atmospheric Administration, and U.S. Department of Commerce. 2005. *NCEP North American Regional Reanalysis (NARR)*. Boulder, CO: Research Data Archive at the National Center for Atmospheric Research, Computational and Information Systems Laboratory. http://rda.ucar.edu/datasets/ds608.0/ (accessed February 2014).

NSIDC (National Snow and Ice Data Center). 2016. *Sea Ice Index*. Boulder, CO: National Snow and Ice Data Center. http://nsidc.org/data/seaice_index/.

NWCC (National Water and Climate Center). 2016a. *About SNOTEL and Snow Courses*. Portland, OR: Natural Resources Conservation Service, National Water and Climate Center. http://www.wcc.nrcs.usda.gov/snow/about.html.

———. 2016b. *Snow Surveys and Water Supply Forecasting*. Portland, OR: Natural Resources Conservation Service, National Water and Climate Center. http://www.wcc.nrcs.usda.gov/factpub/sect_4b.html.

Polar Meteorology Group. 2016. *The Arctic System Reanalysis (ASR)*. Columbus, OH: Ohio state University, Byrd Polar Research Center. http://polarmet.osu.edu/ASR/.

Rienecker, M. M., M. J. Suarez, R. Gelaro, R. Todling, J. Bacmeister, E. Liu, M. G. Bosilovich, S. D. Schubert, L. Takacs, G.-K. Kim, S. Bloom, J. Chen, D. Collins, A. Conaty, A. da Silva, et al. 2011. MERRA: NASA's Modern-Era Retrospective Analysis for Research and Applications. *Journal of Climate* 24:3624–3648, doi:10.1175/JCLI-D-11-00015.1.

Serreze, M. C. and R. G. Barry. 2011. Processes and Impacts of Arctic Amplification: A Research Synthesis.*Global and Planetary Change*, 77:85–96.

Sturm, M. 2012. Ice-Road Trucker Lessons in How Climate Change Actually Impacts Socio-Economic Systems. Seminar presented at CRREL, 24 October. Hanover, NH: U.S. Army Engineer Research and Development Center.

Appendix A. Supporting Data

Snow-Depth-to-SWE Ratios at NWS Weather Stations from COOP Data

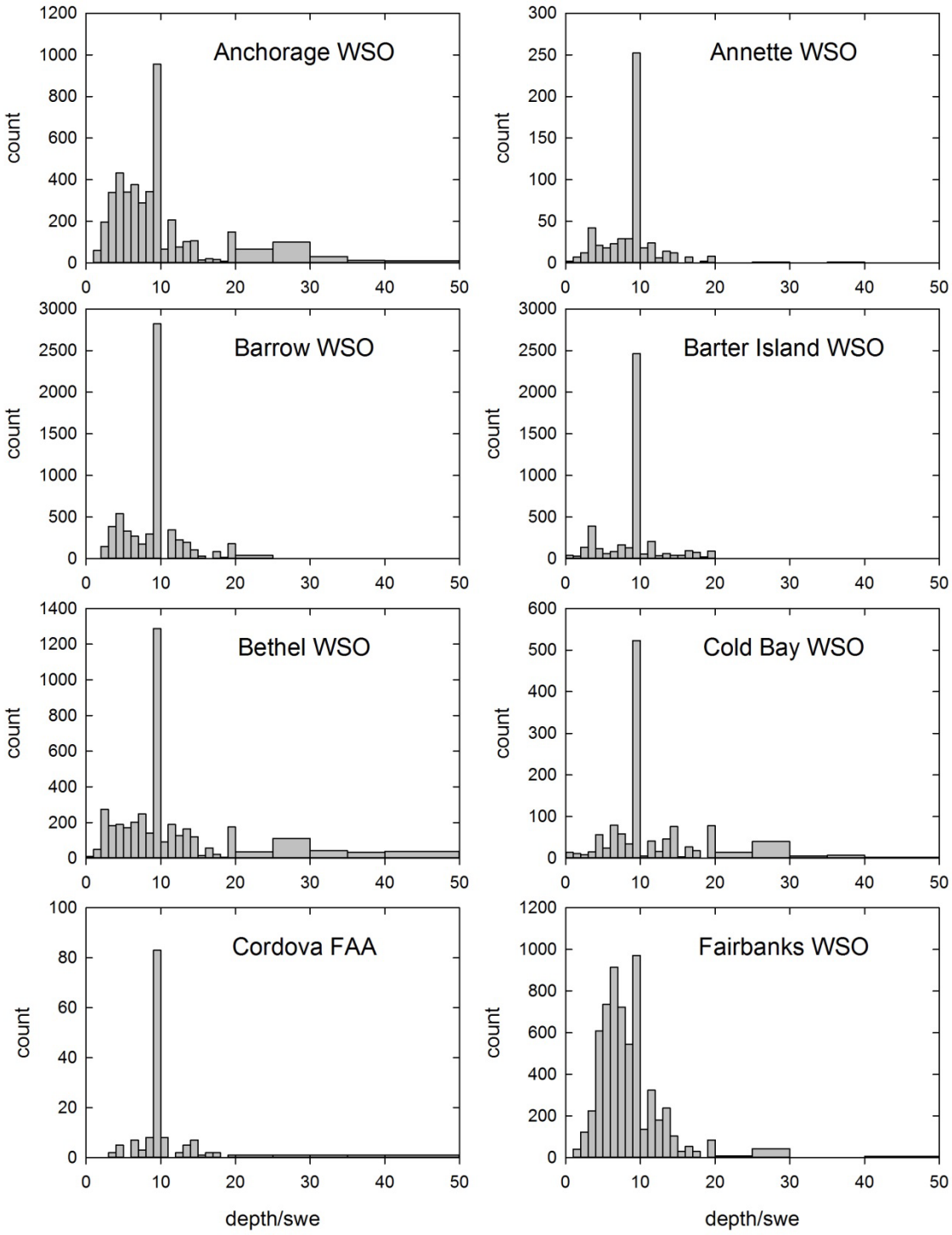

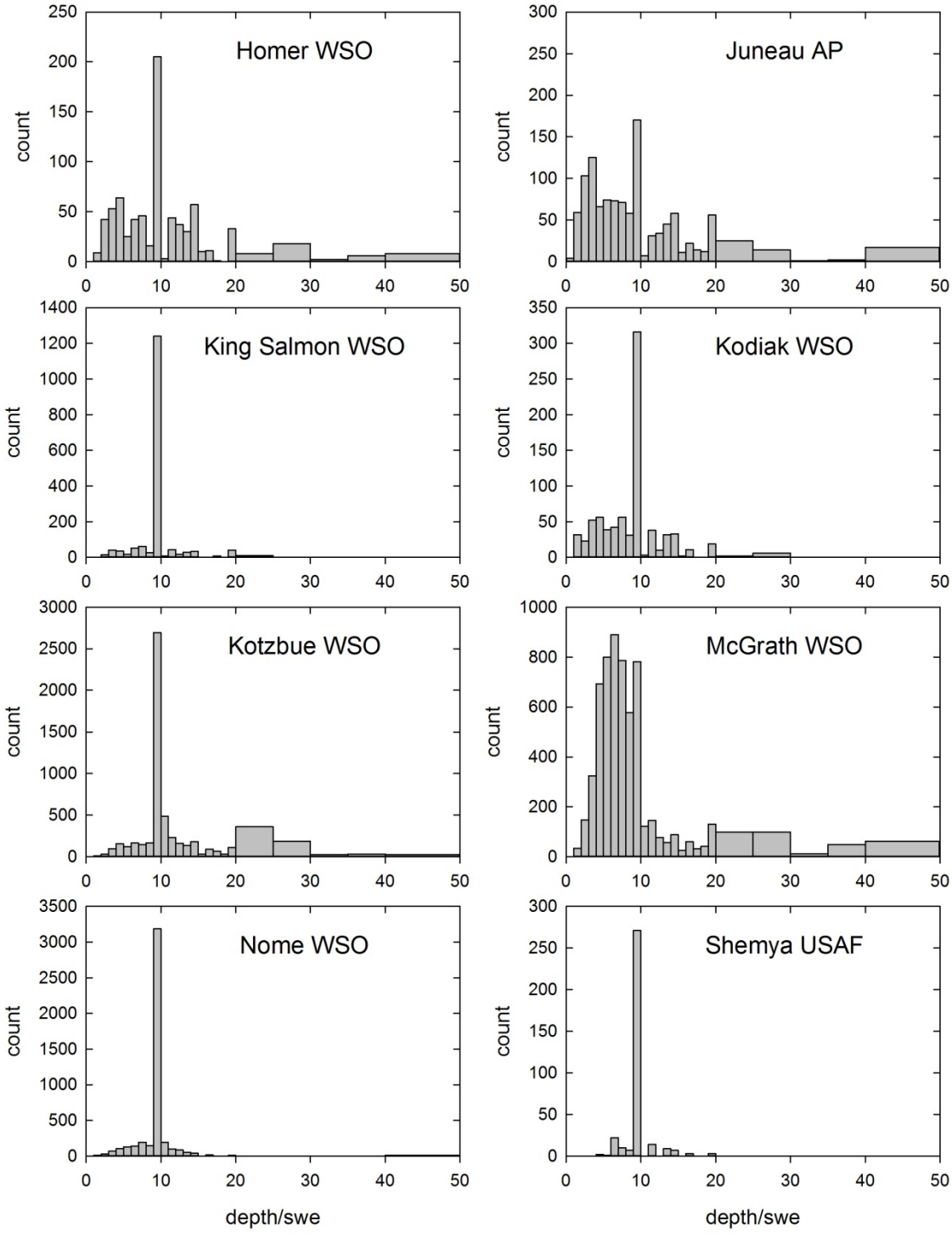
Homer WSO
Juneau AP
King Salmon WSO
Kodiak WSO
Kotzbue WSO
McGrath WSO
Nome WSO
Shemya USAF
count
depth/swe

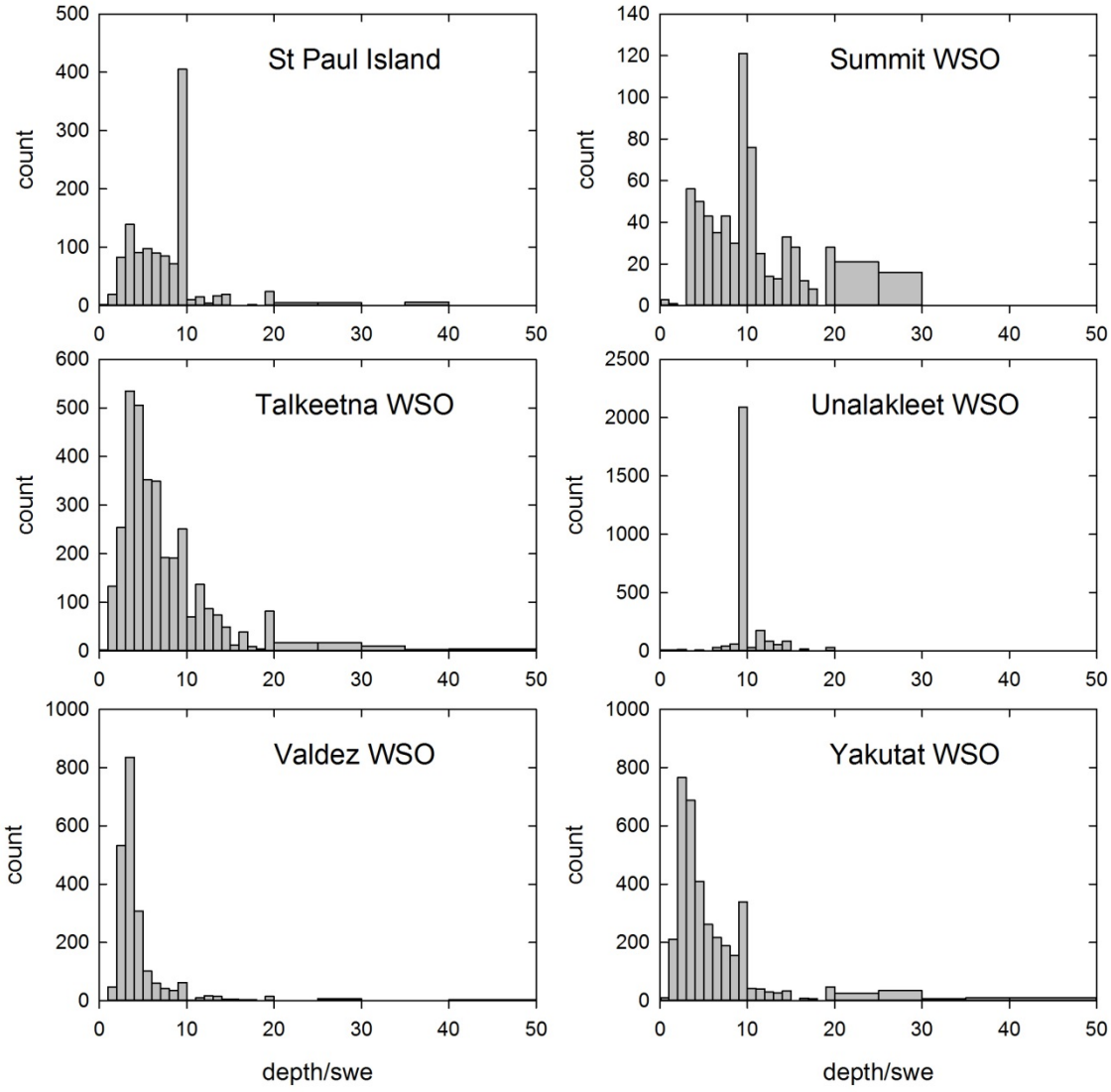
St Paul Island
Summit WSO
Talkeetna WSO
Unalakleet WSO
Valdez WSO
Yakutat WSO
count
depth/swe

Synthetic Data

Synthetic SNOTEL, NARR, and PASR daily SWE data are provided for the pre-AA era and the AA era as sheets in an Excel file SyntheticSWE_SERDP-RC2435.xlsx. There are six sheets altogether (two eras, three datasets). Each sheet has 499 years of SWE data for each location with the era and dataset named on the tab for the sheet. The years are named 4001 through 4499 for both eras. SWE begins to accumulate on day one of each winter year. The winter years are all 365 days long. Each location is a column in the sheet. SWE is given in inches.

Appendix B. List of Scientific/Technical Publications

None

Appendix C. Other Supporting Materials

None

REPORT DOCUMENTATION PAGE

Form Approved
OMB No. 0704-0188

1. REPORT DATE (DD-MM-YYYY)	**2. REPORT TYPE**	**3. DATES COVERED** (From - To)
September 2016	Final	

4. TITLE AND SUBTITLE

Effect of Arctic Amplification on Design Snow Loads in Alaska: SERDP RC-2435

5a. CONTRACT NUMBER

5b. GRANT NUMBER

5c. PROGRAM ELEMENT NUMBER

6. AUTHOR(S)

Kathleen Jones and Steven Daly

5d. PROJECT NUMBER
SERDP RC-2435

5e. TASK NUMBER

5f. WORK UNIT NUMBER

7. PERFORMING ORGANIZATION NAME(S) AND ADDRESS(ES)

U.S. Army Engineer Research and Development Center (ERDC)
Cold Regions Research and Engineering Laboratory (CRREL)
72 Lyme Road
Hanover, NH 03755-1290

8. PERFORMING ORGANIZATION REPORT NUMBER

ERDC/CRREL MP-16-1

9. SPONSORING / MONITORING AGENCY NAME(S) AND ADDRESS(ES)

Strategic Environmental Research and Development Program (SERDP)
4800 Mark Center Drive, Suite 17D08
Alexandria, VA 22350-3605

10. SPONSOR/MONITOR'S ACRONYM(S)
SERDP

11. SPONSOR/MONITOR'S REPORT NUMBER(S)

12. DISTRIBUTION / AVAILABILITY STATEMENT
Approved for public release; distribution is unlimited.

13. SUPPLEMENTARY NOTES

14. ABSTRACT

The Department of Defense seeks an improved understanding and capacity to respond to potential climate change impacts on built infrastructure in Alaska. Other studies have hypothesized that Arctic amplification, the rapid warming of the Arctic compared to the northern hemisphere, causes more persistent weather patterns at midlatitudes, which increase the probability of extreme weather due to drought, flooding, cold spells, and heat waves. Annual maximum snow loads, resulting from the accumulation of snow throughout the winter season, may be strongly influenced by persistent weather patterns. We investigated the effects of these persistent weather patterns on annual maximum snow loads and the resulting design snow loads for buildings.

15. SUBJECT TERMS
Alaska, Arctic amplification, Climatic changes, Extreme value analysis, Load factor design, Snow loads, Snow--Measurement, Snow water equivalent, Structural design, SWE

16. SECURITY CLASSIFICATION OF:			**17. LIMITATION OF ABSTRACT**	**18. NUMBER OF PAGES**	**19a. NAME OF RESPONSIBLE PERSON**
a. REPORT	**b. ABSTRACT**	**c. THIS PAGE**			**19b. TELEPHONE NUMBER** (include area code)
Unclassified	Unclassified	Unclassified	SAR	71	